



TECHNISCHE
UNIVERSITÄT
WIEN

Unterschrift des Betreuers

DIPLOMARBEIT

Analysis of three-dimensional in vitro tissue models using a
light scattering biosensor

Thema

Ausgeführt am Institut für

E163 Institut für angewandte Synthesechemie

der Technischen Universität Wien

Univ. Prof. Dipl.-Ing. Dr. Peter Ertl
Dr.nat.techn., Mario Rothbauer, MSc

unter der Anleitung von

durch

Gregor Höll, BSc

Name

Max Winter-Platz 32/3, 1020 Wien

Anschrift

Datum

Unterschrift (Student)

Contents

Aim of Thesis	ii
Abstract	iii
Acknowledgments	iv
1. Introduction	1
2. Physical Background	10
3. Methods and Materials	13
3.1. Cell Culture	16
3.2. Chip Production	17
3.3. Chip Loading	21
3.4. Experiment Design	24
3.5. Light Scatter Station	27
3.6. Data Acquirement and Output	29
4. Results and Discussion	31
4.1. Characterization of Light Scatter System for 2-dimensional and 3-dimensional Cell Analysis	31
4.1.1. Influence of Laser Power on Light Scattering	32
4.1.2. Influence of Cell Density on Light Scattering	33
4.2. Impact of TNF- α on 2-dimensional Lining Layer Formation on Chip . . .	36
4.3. Measurements of 3-dimensional Micromasses	43
4.3.1. Impact of TNF- α on 3-dimensional Micromass Formation on Chip	47
5. Conclusion	52
A. Materials and Methods	63

Aim of Thesis

In this thesis the adaptation of a previously characterized light scatter station for cell analysis is conducted. A non-invasive method for monitoring of onset and progression of rheumatoid arthritis is developed, allowing further on-chip *in vitro* experiments (e.g. drug efficacy) on the disease in an encapsulated environment in the future.

Abstract

About 1% of the world's adult population suffers from rheumatoid arthritis, enduring pain and disability, as these are the hallmarks of this chronic joint inflammation. As no cure has been found yet, research into this highly complex disease is needed. Fibroblast-like synoviocytes have been discovered as one of the key players as they are crucial for synovial lining layer formation which leads to cartilage and bone degradation.

By culture of synoviocytes in a 3-dimensional Matrigel matrix on chip, lining layer formation similar to *in vivo* could be achieved. Coupling of these micro-scaled biochips with non-invasive light scattering enabled the time-resolved analysis of rheumatoid arthritis in its early stage.

Light scatter measurements as complimentary insights in parallel with microscope images revealed that the inflamed condition, induced *in vitro* by administration of tumor-necrosis-factor- α , yields higher cell proliferation, increased production of adhesive molecules and a more dense lining layer formation than healthy, untreated synoviocytes. Thus this powerful *in vitro* technique confirms what has already been reported in literature for *in vivo*, therefore making it a promising tool for further research, as it offers the ability to rapidly screen drug impact on rheumatoid arthritis.

Acknowledgments

First of all, I want to thank my Professor, Univ. Prof. Dr. Peter Ertl for the opportunity to work in his Cell Chip Group on such an interesting and important topic. Even as vital for my thesis, as well as scientific and personal development, were Dr. Mario Rothbauer and the rest of the group. By them I was introduced to the fields of Microfluidics, Biology, Medicine, Yogurt and Bureaucracy, polishing not only my CV but also getting an understanding of the working environment in a laboratory.

In the course of my studies I worked with many people who helped, pushed and enabled me along with my friend and family, and for this I am deeply grateful.

Least but first, I want to thank my parents for their support enabling an academic education and more than anything for their unending patience.

1. Introduction

Inflammation is an integral part of the complex biological response to harmful stimuli (e.g. pathogens, trauma, cell damage) and is a protective response of the human body involving immune cells, vessels, and biochemical cues. During infection for instance different types of cells and a broad palette of cytokines regulating growth and differentiation of cells come together to achieve tissue repair. Among cell types important for effective wound healing fibroblasts help wound closure due to secretion of collagen, which is an important structural protein tissues are built of. Further, chemical mediators such as tumor necrosis factor- α (TNF- α) tightly control and enhance inflammatory responses by B and T cell activation [1]. Although part of the natural healing process and regeneration in the human body, inflammation also plays a key role in onset and progression of human diseases such as metabolic disorders including obesity and diabetes type 2 [2]. Furthermore, chronic inflammation is also connected to cancer progression [1].

Onset and Progression of Rheumatoid Arthritis Among human diseases Rheumatoid Arthritis (RA) is a chronic autoimmune disease involving inflammation of mostly small joints in hand and feet, however, other joints can also be affected. Occurrence of RA is estimated to be around 1.0% of the global adult population [3],[4] with a 200% higher occurrence in female patients and onset at a critical age around 30 to 55 years [5]. Although the cause for RA is still unknown, genetic disposition has been cleared as the sole reason because studies with monozygotic twins show disease outbreak in both test subjects only in 12-15% of the cases [6],[7].

To understand the progression of RA it is important to investigate the anatomical differences between joints of healthy compared to arthritic condition as shown in figure 1. Normal synovial tissue consists of a top lining layer with a thickness of one to two cell layers covering connective tissue which is referred to as sub-lining and is responsible for lubrication and nutrient supply of cartilage [9],[10]. Two important cell types in hu-

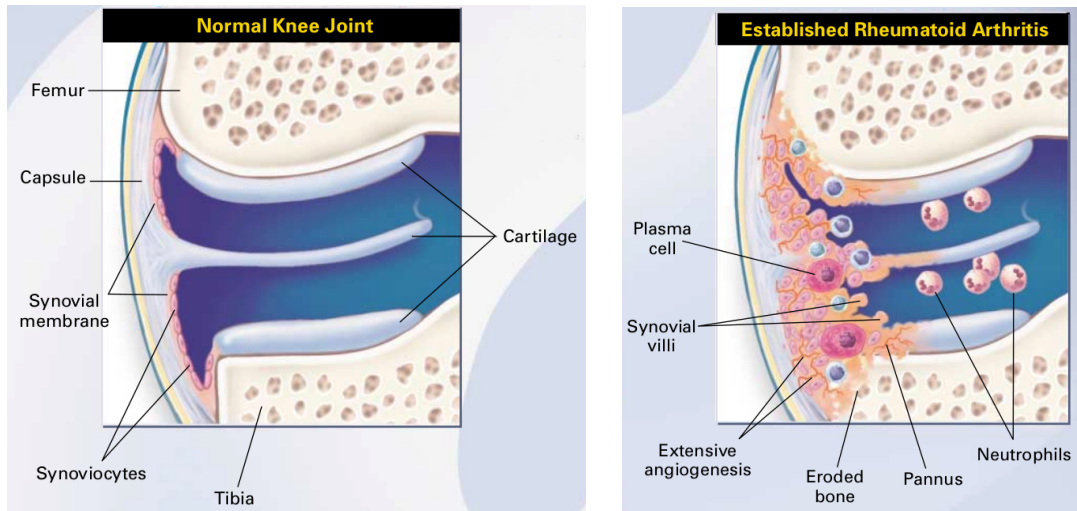


Figure 1: Knee joint in healthy condition and with established rheumatoid arthritis. Hyperplasia of the synovial membrane with a thickened lining layer, the inflammatory tissue (pannus) and angiogenesis are visible. Adapted from [8]

man synovium are macrophage-like synoviocytes (MLS) and fibroblast-like synoviocytes (FLS). While macrophage-like synoviocytes behave like other macrophages clearing debris and watching out for pathogenic entities, fibroblast-like synoviocytes are involved in the production of extracellular matrix (ECM), lining layer formation as well as secretion of lubricating agents into the joint cavity [11],[12].

In the underlying sublining various other cell types are present including mostly T cells, but also other immune cells such as B cells, dendritic cells and macrophages [11] (see figure 2). During onset and progression of RA, inflammatory processes result in thickening of the lining layer up to 20 cell layers due to an increase in both major resident synovial cell types [13] being referred to as synovial hyperplasia or synovial fibroblast hyperplasia.

Three major contributing factors for development of a hyperplasia of the synovial lining layer are enhanced synoviocyte proliferation, reduced apoptosis and cell recruitment from outside the synovium. Increased proliferation, caused by a mixture of growth

factors, chemokines (proteins which cause cell movement) and cytokines (e.g. $\text{TNF-}\alpha$), leads to a gain in synoviocyte cell number [14],[12]. Whereas mutations in tumor suppressor gene p53 in cells with DNA damage result in reduction, or even inhibition, of apoptosis [15]. To provide enough cell material for the increased cell mass present in synovial hyperplasia, cell recruitment from other sources, outside of the synovium, like the bone marrow [16] is required and facilitated by fibroblast-like synoviocyte migration due to chemokines [14],[17],[18].

In contrast, cell to cell interaction of fibroblast-like synoviocytes within the sublining layers results not only in immune cell recruitment, activation and extensive angiogenesis but also in differentiation and retention of sub-lining cells [8],[14]. On a tissue scale these inflammatory processes that cause synovial hyperplasia result in formation of a pannus which invades the joint cartilage [19] as shown in figure 2. Again, fibroblast-like synoviocytes are a key player in this process as they not only facilitate invasion, but also production of cytokines and bioactive substances such as (cartilage-) matrix degrading enzymes [20] (also see table 1).

Table 1: FLS activators and products, including pro-inflammatory compounds and degradative enzymes. Adapted from [14].

FLS Activators	FLS Products
Cytokines: TNF- α , IL-1 β , IL-6, IFN- γ	Cytokines: IL-6, TNF- α , IL-1 β
Growth Factors	Growth Factors
Chemokines	Chemokines
Cell Surface Ligand Interactions	Cell Surface Receptors: VCAM-1, ICAM-1
Tissue Degradation Products Thrombin Fragments	Degradative Enzymes: MMPs, cathepsins
Hypoxia	

These enzymes result in destruction of the joint cartilage and subsequently of the underlying bone in late stage RA. For the synoviocytes to begin degradation of cartilage, the

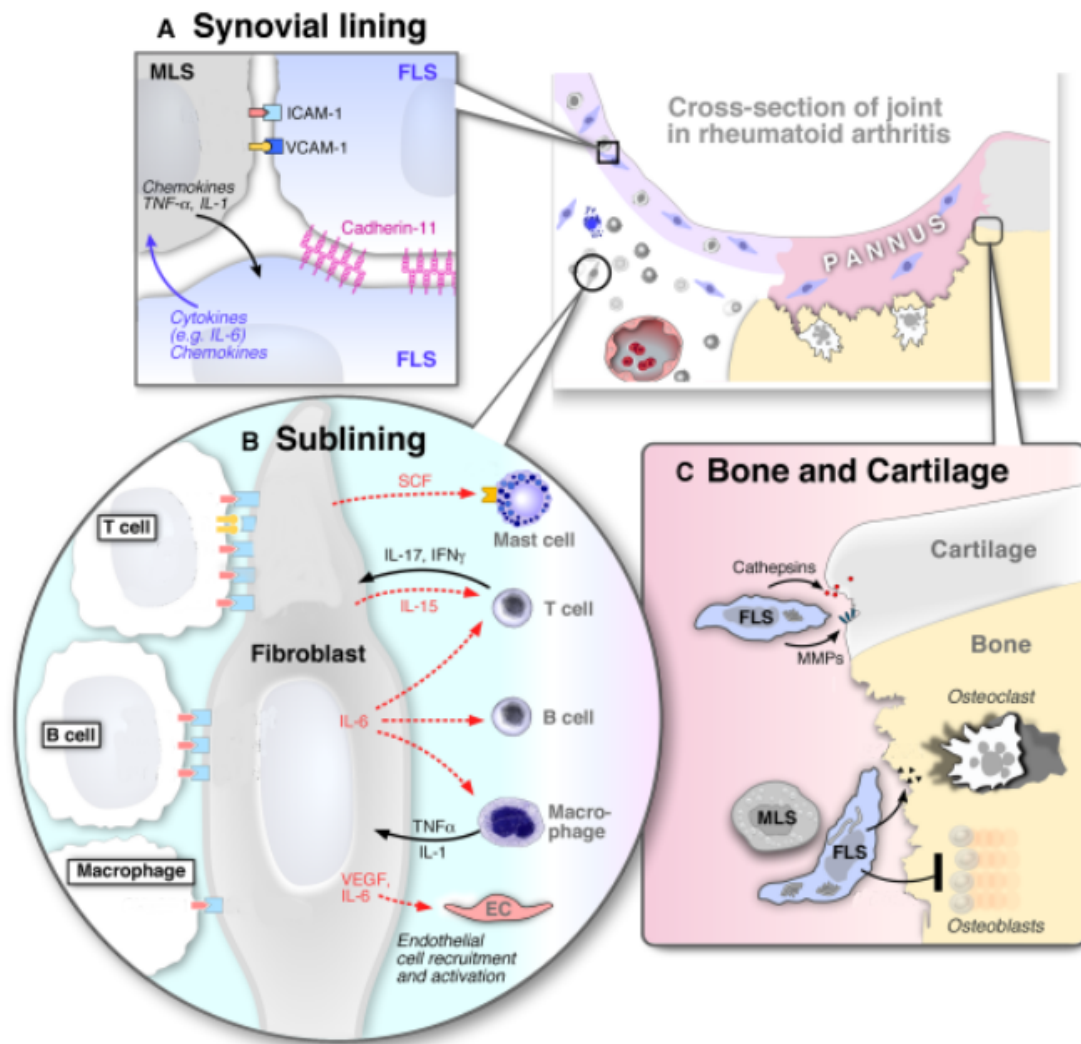


Figure 2: A) Interactions between synoviocytes in the lining layer are guided by multiple sources, including chemokines, cytokines (e.g. TNF- α , IL-6) and cell adhesion molecules. Cadherin-11 is especially important for cell to cell linkage of FLS. B) In the sub-lining manifold processes between fibroblast-like synoviocytes and other cells, such as T cells, B cells and macrophages occur. C) Formation and invasion of synoviocytes (MLS and FLS), in the form of a pannus, into joint cartilage and bone are facilitated by the production of degradative enzymes (e.g. MMPs). Other FLS products support osteoclast differentiation and activation while stopping osteoblast function. Adapted from [14].

cells initially need to attach to the cartilage matrix. This important process is guided by integrins, which facilitate matrix metalloproteinase (MMP) expression, another class of degradative enzymes that is responsible for ECM breakdown. Other adhesion molecules involved are intercellular-adhesion-molecule 1 (ICAM-1) and vascular-adhesion-molecule 1 (VCAM-1). The role of the latter regarding FLS adhesion to cartilage has already been shown in animal studies, whereas cytokine induced ICAM-1 expression has been reported for fibroblasts [13]. Furthermore, VCAM-1 stimulates the chemokinetic behavior of T cells in RA [21]. Aside from ICAM-1 and VCAM-1 also Cadherin 11 is important for buildup of the synovial lining, adhesion to cartilage, enhanced cell invasiveness as well as alteration in cell to cell interaction among individual synoviocytes [13],[22].

Strategies for Establishment of Physiologically Relevant RA Models In Vitro Many treatment strategies for RA directly target the immune system, however, to achieve more control over RA progression, still more potent medications need to be tested. As example, anti-TNF- α and -IL-6 agents have been used as treatment strategy to slow down the progression of RA, however, increasing the risk of infection for RA patients [14],[23],[24],[25],[26]. As no effective cure has yet been found, further research needs to be performed. Especially, synoviocytes as key player in RA is believed to generate promising results to understand this complex pathological process since synoviocytes *in vitro* can be stimulated biochemically via for instance TNF- α to induce RA phenotype [27]. Even though extensively used throughout the last eight decades, *in vitro* models based on 2-dimensional cell culture models are still used for many aspects (e.g. cell cultivation, toxicology, biocompatibility studies, etc.), limitations are evident. Nowadays, to perform cell-based assay with increased *in vivo*-like relevance for human biology and pathophysiology, cells need to be maintained and exposed to a suitable, *in vivo*-like microenvironment that resembles tissue architecture. 2-dimensional *in vitro* experiments, which are normally performed prior to animal and clinical tests, often lead to question-

able results that are not comparable to those *in vivo*. About 90% of clinical trials in drug discovery fail, which is very time consuming and of course creates vast economic burden. Therefore, 3-dimensional cell culture methods and models are needed and sought after to minimize risks and costs during drug development and clinical trials. Spherical agglomerates of cells, so-called spheroids or organoids, are cell-based assemblies that show gradients of oxygen and nutrients that resemble those found in native tissue [28]. Studies regarding RA using synoviocytes pointed out limitations of monolayer cultures compared to 3-dimensional models [29]. More striking differences can be seen when comparing architectural aspects. Monolayer cultures for instance cannot generate a synovial lining layer neither for healthy nor diseased synovium. Here, 3-dimensional micromasses comprising of synoviocytes embedded in an ECM extracted biopolymer show superior performance on a functional level, since biochemical and biophysical gradients guide cell migration and the separation of lining from sub-lining over a time course of several days and weeks [30]. Aside from methods that use cellular self-assembly to generate 3-dimensional models, natural as well as synthetic hydrogels are extensively researched and applied for tissue engineering and biomedical applications (see figure 3 for concepts of using a matrix for cell culture). Based on different biochemical and physical principles, these 3-dimensional hydrogels often need different cross-linking means to build up the matrix, including enzymes, molecular functional groups, temperature change and others. Once the hydrogel is polymerized supply of nutrients, biomolecules or stimulants into the gel is possible due to the high content of water [31].

Rüger et al for instance used a fibrin-(protein connected to clotting process of blood)-based 3-dimensional matrix to study the connection of vascularization and inflammation [32]. Zheng et al researched the migration of cells through a Matrigel membrane [33]. Matrigel, a basement membrane extract produced by Engelbreth-Holm-Swann mouse tumor cells [34], has already been used in combination with synoviocytes. Culture and migration of synoviocytes through Matrigel was done by Hardy et al [35]. Importantly

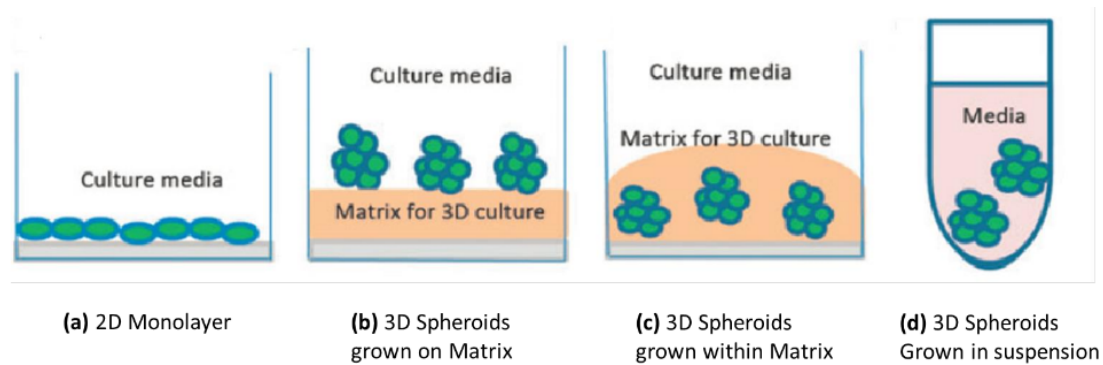


Figure 3: Schematic representation of a) cells in a 2-dimensional monolayer, b) 3-dimensional spheroids/aggregates on a matrix, c) 3-dimensional spheroids/aggregates within a matrix, d) 3-dimensional spheroids/aggregates in suspension [28].

it has been reported that Matrigel resembles the natural ECM in synovial tissue [30] making this particular hydrogel type a promising and feasible choice for research on RA.

Non-invasive Optical Biosensing Method for Continuous Measurement There are many definitions of biosensors, one of them is the following:

”A biosensor is an analytical device incorporating a deliberate and intimate combination of a specific biological element (that creates a recognition event) and a physical element (that transduces the recognition event).” [36]

The biological element corresponds to the behavior of cells (e.g. growth, adhesion, network formation, apoptosis, necrosis, etc.). Choosing an appropriate physical element however is not so simple, as there are many physical properties that can be used for a biosensor including optical, magnetic and electrochemical principles. Most commonly used, however, are optical biosensors [37] and can be further divided into two groups, the ones which use a label (label-based) like fluorescence and absorbance, and the ones that do not (label-free) like chemiluminescence and light scattering. All of these sensing methods measure similar parameters which is a change in light intensity [37], [38].

Alternative optical biosensing techniques rely on a close proximity of the biosensor to the biologic sample (e.g. surface plasmon resonance) [37], however, the synoviocyte lining layer is a process that happens within a 3-dimensional context in native tissue [10],[39],[30]. Therefore, these cannot provide necessary spatial resolution. The decision whether a label-based or label-free method is better suited for this complex task is difficult. On the one hand, label-based methods have shown their merits and the most commercially successful biosensor, the handheld analysis device for blood sugar (glucose) in diabetes patients, is belonging to this group [37]. However, continuous measurement of a sample is often necessary to get an insight into temporal changes on a cellular level during inflammatory processes such as RA. When interaction between label and cells to be tested, which could possibly even influence the biological outcome, is unwanted less invasive label-free approaches may be more applicable. Light scattering in particular is not a new technique per se and has already proven its worth in many studies. Raschke et al already used it in 2003 for the detection of specific biomolecules [40] and Goldberg showed the ability of light scattering to study Brownian motion in fluids [41]. Bi et al showed light scattering as a versatile biosensor for nucleic acids and proteins [42]. The versatility of light scattering for the detection of different sizes and distributions of nanoparticles [43] is one huge advantage, as the size and distributions of not only synoviocytes but also their organelles and network can be of potential great interest. A combination of light scattering and confocal light absorption has already shown the ability to non-invasively detect internal cell structures [44]. As also cell shape and orientation have an impact on the signal as Watson et al reported [45], light scattering is a qualified technique for the spatio-temporal analysis of complex cellular behavior.

Organic Photodiodes as Optical Biosensor for Cell Analysis Once the light comes in contact with a biological region of interest, biological processes may lead to structural or morphological rearrangements and remodeling, which in turn results as differences in

scatter behavior. Therefore, scattered light as analogue signal has to be collected efficiently, converted into a digital signal and further analyzed using data analysis software. For detection of light - scattered or not - many strategies can possibly be used including photodiodes, photomultiplier tubes or charged coupled devices.

In recent years, however, organic photodiodes (OPD) have shown promising results in combination with notch filters for light scattering applications. OPDs are organic semiconductors that have similar sensitivity as photomultiplier tubes and charged coupled devices. Furthermore, low fabrication costs and the multitude of possible substrate materials makes them superior to silicon-based diodes [46]. Additionally, organic photodiodes allow good photo-regeneration yield, low temperature processes and effective light absorption over large areas of the light spectrum [47]. Tedde et al used spray coated OPDs and reported high sensitivity and shelf life [48]. Organic photodiodes displayed simple alignment and an exact shape control of the photoactive area [49]. Charwat et al also reported a non-invasive long-term cell analysis method by coupling detection of scattered light by an OPD with an electrode array on a Lab-on-a-chip device [50].

Microfluidics Technology for Miniaturization and Automation of Cell-Based Assays

Microfluidics and Lab-on-a-chip (LOC) systems offer the opportunity to cultivate *in vitro* cell cultures within a highly controllable micro-scaled liquid environment for experiments that require small amounts of compounds and precise control of spatial and temporal dynamics of the cellular microenvironment [51]. Especially since bioavailability of patient samples thus primary cell samples is low, efficient use of such scarce resources by reduction of cell numbers necessary for a individual test run is very important. The impact and rise of microfluidics since the year 2000 has been reported and the combination of optical detection and microfluidics is used by an increasing number of research groups [38],[51]. Light scattering for particle detection and cell interactions [50],[52] offer a good basis for analysis of fibroblast-like synoviocytes. Microfluidic chips offer on

one hand quantitative data acquisition in real time with high sensitivity [49]. Additionally, low cost chip fabrication allows good scalability and multiplexing of experiments [38] which is required especially for experimental set-ups dependent on rare or scarce primary tissue samples.

The ability to miniaturize and integrate automated biomedical assays supports microfluidics as promising and emerging technology to advance today's state-of-the-art cell-based assays for biomedical research [53]. The latest advancement to refine such systems was made by combination of microfluidics and lab-on-a-chip systems with 3-dimensional tissue engineered organ models on micro engineered chips which allowed the rise of organ-on-a-chip technology as the next generation of cell-based assays for drug development [54]. These intricate and highly engineered systems aim to reduce the need animal tests for pharmaceutical research and to get more insight into the human body on the organ and tissue level. However, as promising the idea behind body-on-a-chip system may sound, further research has to be conducted validating these methods [55]. Nevertheless, microfluidics came to stay as valuable toolset for biomedical research.

2. Physical Background

Interactions of light with other media is governed by fundamental principles, including reflection, diffraction, refraction and scattering. Due to the measurement set-up used in this thesis only forward light scattering with angles greater than 20° is of interest, and therefore light scattering will be described in a phenomenological approach in this section.

Light scattering cannot be seen as the mere collision of light particles (photons) with an object, because light not only has particle but also wave characteristics. This, combined with its involvement with electric and magnetic fields, lead to its labeling as electromagnetic wave (EM wave). Scattering is due to interaction of an incident EM wave with a volume of different properties (e.g. density) [56]. To be precise, the scattered volume,

for instance a particle, consists of atoms containing electrons moving around them in orbits. These electrons are excited by the incident EM wave and start oscillating with the frequency ν_0 of the incident wave. Due to the charge separation a dipole moment is induced [57], which leads to formation of a new EM wave in the form of scattered light, see figure 4.

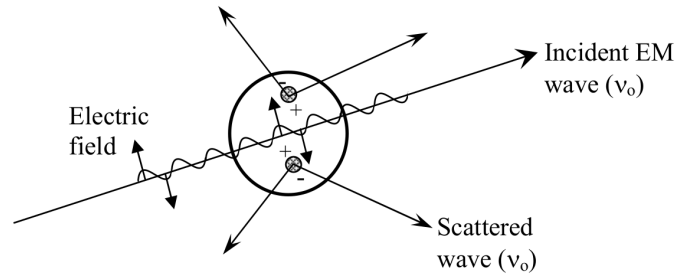


Figure 4: Schematic representation of light scattering by an induced dipole moment due to an incident EM wave [57].

As the exact numeric calculation of light scattering is very complex and requires tremendous amounts of computational power, simplified theories have been developed as a generalization. Mie-scattering is such a theory and concentrates on the description of interactions of light with spherical particles and is widely used, when the particle size is in the range of the incident wavelength or larger. In this case different electric dipole moments will be excited in the particle which are out of phase with each other, leading to a superposition of scattered EM waves. An angle dependent strength of the scattered light intensity is due to this superposition, where forward scattering is favored with a maximum in the direction of the incident light [58].

For usually used light sources light scattering of mammalian cells is in the regime of Mie-scattering [60]. However, not only the cell itself but also structures inside of cells have to be regarded as potential scattering candidates. Mourant et al reported that the bulk of scattering in mammalian cells like fibroblasts is due to the structures within the cell. In contrast to particles in the size range of cells, which favor forward scattering,

cell organelles and their structures, depicting a size much smaller, show larger scattering angles [61].

Rayleigh-scattering can be applied if the scattered particle size is small compared to the wavelength of the incident light, which is $\alpha \ll 1$ for α in equation 1.

$$\alpha = \frac{\pi d}{\lambda}, \quad (1)$$

where d is the particle diameter and λ is the relative scattering wavelength, which takes the refractive index of the medium around the particle in account. In this case, combined with elastic scattering for spherical particles, Mie-scattering is reduced to the further simplified Rayleigh-scattering, in which particles exhibit a uniform electric field at any given time resulting in dipole moments which are in phase with each other [57]. Therefore, the angular distribution of the scattered light is broader than for Mie-scattering, as can be seen in figure 5.

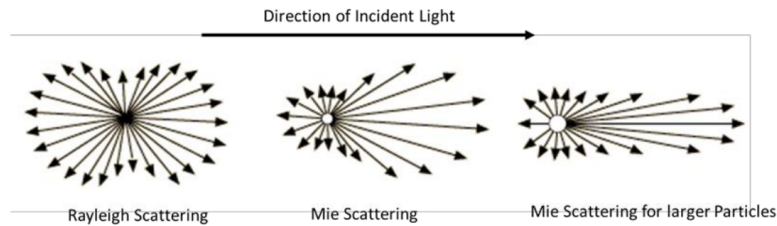


Figure 5: Schematic of scattering behavior in different regimes [62].

For a single ray of unpolarized incident light the scattered intensity in Rayleigh-scattering can be calculated with

$$I_{scat} = I_0 \frac{1}{r^2} \sigma'_{scat}, \quad (2)$$

where I_0 is the intensity of the incident light, r the distance from scatter- to measurement-event and σ'_{scat} the differential scattering cross section, which accounts for the angular scattering distribution [57].

In order to calculate light scattering of a sample one needs to modify equation 2 with an absorption term and account for multiple scattering events of single rays with particles in different size regimes and a shape distribution beyond spherical ones. For a biological sample the light scattering will take place in Mie- and Reyleigh-regimes due to different sizes of cells, organelles and their structures and therefore, both will be detected in a measurement. Technically, Mie- and Reyleigh-scattering are only valid for spherical scattering particles, however, studies showed that they can be used as an approximation. Steinke et al compared light scatter measurements of red blood cells with theoretical calculations according to Mie-scattering. Although the disk-like shape of the cells gave cause to some differences, they found that results from theory and experiments fit quite well overall, indicating that the volume of the particle is more important than it's shape [59].

3. Methods and Materials

For convenience all used components are displayed in table 2 (equipment) and 3 (consumables).

Table 2: List of the used equipment for measurement station set-up and experiments.

Component	Manufacturer	Cat. No
Biopsy puncher	Stiefel	01.SF003.01/15 05
Centrifuge	Eppendorf	Centrifuge 5430
CoolCell	Biocision	BCS-405G
Drill	Komet Dental	805 314 009
Fluorescence Microscope	Olympus	IX83
Microscope	Olympus	IX71
Multimeter	Iso-Tech	IDM67
Neubauer-Improved	Marienfeld	0640010
Neutral Density Filter	Thorlabs	ND20A
Notch Filter	Melles Griot	Specifications of 03FIN-series
OPD	Siemens	Siemens Design
Plasma cleaner	Harrick Plasma	PDC-002-CE
Plate Reader	PerkinElmer	Enspire 2300
Plotter	Roland	Camm-1 GS-24
Powderblaster	Logiblast	Corn size of 120 μm
Powermeter	Coherent	LaserCheck
Sapphire 488-75	Coherent	LDP.1116054.091969
Water Bath	Grant	GLS400
Water Bath Pump	Julabo	Julabo 4

Table 3: List of the used consumables for chip production and cell culture.

Component	Manufacturer	Cat. No
Adhesive PCR Seal	Sarstedt	95.1993
Adhesive Tape	Adhesive Research	ARcare 90445/90445Q
Antibiotic Antimycotic Solution	Sigma	A5955-100ML
Calcein	Invitrogen	L3224
DMEM	Sigma	D5796-500ML
DMSO	AppliChem	A3608,0500
Ethidiumhomodimer	Invitrogen	L3224
FBS	GE HC Life Sciences	SH30070.03
Glassslide	VWR	631-1550
Hellmanex	Sigma	Z2805939-1EA
HEPES	Amresco	J848-100ML
Insulin-Transferrin-Selenium	gibco	41400-045
Low Temperature Freezer Vials	VWR	479-1254
L-Ascobic Acid	Sigma	A5960
Matrigel	Corning	354230
MEM Non-essential Amino Acids	gibco	11140-050
PBS	Sigma	D8537-500ML
PDMS	Dow Corning	Sylgard 184
PolyHEMA	Sigma	P3932, 10G
Sandblast foil	Gemba	Sanblast Super
Sugru	Sugru	I000469
Syringe (1ml)	Becton Dickinson	300013
S-Layer	BOKU Wien	Protein SbpA
Trypsin	Sigma	T3924-500ML

3.1. Cell Culture

A protocol for the isolation and culture of fibroblast-like synoviocytes was reported by Zhao et al [63]. Primary cells contributing to this thesis though were provided in culture by the research group of Dr. Kiener, AKH Wien.

Due to sterility all cell culture procedures were performed inside of a laminar flow hood. Cells were provided in culture and were frozen when confluent, if not directly used in an experiment. Growth medium for FLS consisted of DMEM high glucose, 10% FBS, 1% Antibiotic Antimycotic Solution and 1% MEM Non-essential amino acids.

Before freezing cells were split and resuspended. First cells were washed twice with PBS and trypsinated for 6 minutes at 37° C in an incubator. Once thy synoviocytes detached from the surface the cell supernatant mixture was centrifuged for 5 minutes at 1200 rpm. After removal of supernatant resuspension of the cells with 900 μ l growth medium in a cryo vial (low temperature freezer vial) was conducted. Right before putting the labeled vials in a Mr. Frosty freezing container(CoolCell), enabling a temperature drop of 1° C per minute when stored at -80° C, 100 μ l of dimethyl sulfoxide (DMSO) was added. After 24 hour storage in the freezing container, the cryo vials were transferred to a liquid nitrogen tank. Thawing of the cells was done by slowly swirling the cryo vials in a water bath at 37° C until almost all ice melted. At this point the vials were moved inside the laminar flow hood and the content of the cryo vials was pipetted into beforehand prepared falcon tubes containing growth medium. After centrifugation and extraction of supernatant the cell pellets were resuspended in T75 flasks with 10 ml of growth medium. Depending on how many cells were needed or on passaging the cells for further growth, cells were split in a ratio of 1:2 to 1:3. For cells in culture growth medium was exchanged weekly or when cells were split. In case of the latter cell culture flasks were treated the same way as before freezing. After washing with PBS, trypsination and centrifugation the resuspended cells were distributed in T75 cell culture flasks with 10 ml growth medium, which was warmed up in a water bath at 37° C.

Fluorescence live-dead stainings were obtained by incubation of the cells at 37° C for 20 minutes using growth medium containing 0.2% Ethidiumhomodimer and 0.05% Calcein.

When used, TNF- α concentration in medium was set at 10 ng per ml, Interferon- γ at 5 ng per ml.

Coating of 12 well plates was done by using Poly(2-hydroxyethyl methacrylate) (poly-HEMA). 100 mg of polyHEMA was mixed with 10 ml absolute ethanol for one hour just below 100° C in a closed container using a magnetic stirring machine. Once mixed polyHEMA was pipetted into the well plates, which were closed and stored at room temperature for three to four days until the ethanol was evaporated.

3.2. Chip Production

In order to conduct reproducible experiments a standardized chip was developed.

Mold Design

Mold Layout was designed using AutoCAD 2017 and later 3D printed (i.materialise) using grey resin as material for the mold (see figure 6). To maximize data output and save materials the chip consisted of four separated chambers for multiplex experiments. One corner of the mold, and therefore the chip, was set at a different height allowing easier chip handling by using a pair of tweezers (see left bottom corner of 6b).

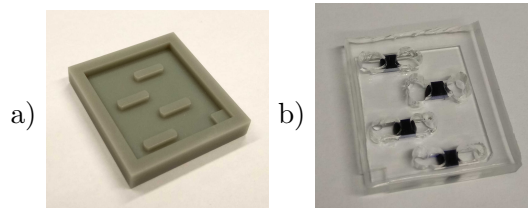


Figure 6: a) Mold for rapid chip production using commercially available grey resin, b) completed chip with blue ink.

A mixture of Polydimethylsiloxane (PDMS) Silicone Elastomer and Silicone Elastomer Curing Agent in the ratio 10:1 was mixed for about 3 minutes. During this process air bubbles occurred in the mixture which was then poured onto the mold which was previously treated with 2% diluted Hellmanex and Isopropanol. Excessive PDMS was removed by smoothing out the surface. The mold with liquid PDMS was then baked in an oven at 70° C for the duration of 1 hour. After the first 5 minutes of the baking process a manual check for remaining air bubbles was conducted. Bubble removal was performed by agitation of the mold onto a flat surface. Baking time varied with the temperature used [64]. As no curing time was given by the manufacturer for 70° C the PDMS was cured for 1 hour at 70° C and then for another 24 hours at room temperature. Once cured, holes were created at the ends of each chamber using a Biopsy puncher with 4 mm diameter. These served as chamber access points once the chip was completed. The PDMS part and a glass slide of appropriate size for the chip bottom was then cleaned by using washing soap, water and Isopropanol. Compressed air and 30 minutes in an oven at 70° C guaranteed the dryness of used materials. Both parts were put into a plasma cleaner with the bonding surface upwards and irradiated with high frequency plasma (30 W) for 2 minutes. Afterwards the plasma activated surfaces were pressed together to bond. To ensure superior bonding clamps were used to press the materials together and all was put into an oven for at least 12 hours at 70° C.

Before usage the chips were sterilized by rinsing with 70% Ethanol. A completed chip with blue ink loaded in the middle chamber is shown in figure 6.

Cylindrical Holes in PDMS

Initial 3-dimensional experiments were conducted using a chip consisting of a PDMS layer (height about 2-3 mm) plasma bonded onto a glass slide (see figure 7a). Prior to the bonding holes for micromass placement were created and PDMS layer and glass slide were washed with washing soap, water and Isopropanol. Cylindrical holes were

produced by the means of a biopsy puncher with a diameter of 2 mm.

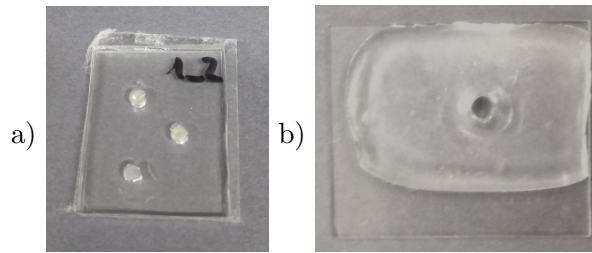


Figure 7: a) PDMS on glass chip filled with fibroblast-like synoviocyte micromasses. b) Empty PDMS on glass chip with a spherical cavity on top of a cylindrical hole.

Semi-spherical Cavity in PDMS

A different chip design was based on the idea to create a small semi-spherical cavity with a cylindrical hole in the middle. Thus the micromass was pulled by gravity to the cavity's center yet not into the hole (see figure 7b). Using a commercial available mouldable glue (Sugru) a mold for PDMS was created with a small spherical indentation. PDMS was cured for one day at 70° C and for one hour at 120° C using this mold. The last step hardened the PDMS thus it could be used as a mold for PDMS itself. With the PDMS-mold, which is the negative of the desired structure, a new PDMS object could be created with the same spherical indentation as the one of the mouldable glue. Before plasma bonding of PDMS to a glass slide the same procedure for production of cylindrical holes and washing was used as for 'Cylindrical Holes in PDMS'.

Pressure-sensitive Adhesive Tape

A more complex chip design based on the usage of inlet and outlet channels for medium and an adhesive tape replaced the function of PDMS on glass bonding. The tape was non-toxic and had an adhesive layer at the top and bottom with a total thickness of 80 μm (Adhesive Tape).

The chip for 2-dimensional experiments (2D-chip) consisted of five layers: glass bottom

as surface for biology, adhesive tape, glass with channel structure, adhesive tape, glass top with holes as inlet and outlet ports (see figure 8a).

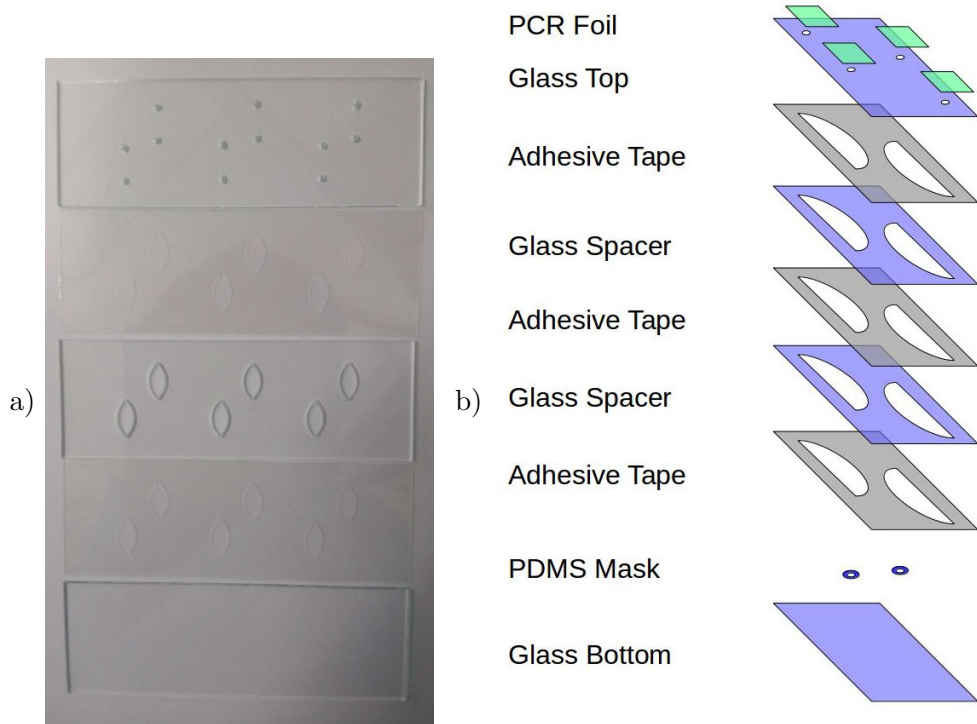


Figure 8: a) Individual parts of 2D-chip with five layers consisting of glass slides and adhesive tape. b) Schematic of individual parts of micromass-chip with nine layer consisting of glass slides, adhesive tape and PDMS mask with a height of 250 μm .

A CAD design was created for every layer, in which the dimensions of all layers were the same (76 mm x 26 mm). By using these dimensions whole microscope slides could be used, and more chambers or bigger medium reservoirs could be achieved on one chip. By the use of a plotter the layout of glass channels was cut into a sandblast foil, acting as a mask for powder blasting. Microscope slides were used as substrate material for the glass channel layers and shaped by a powderblaster with a corn size of 120 μm . Using a 0.9 mm drill holes for inlet and outlet ports were drilled into a glass slide, acting as top layer. All glass layers were then cleaned by using washing soap, water and Isopropanol. The

adhesive tape was cut into the same layout as the glass channels using the same plotter. Later they were placed with one adhesive layer on the glass channels and adhered there. In the final step the bottom glass layer and the top glass layer with holes were placed on the other adhesive surface of the adhesive tap already placed on the glass channels.

Before usage the chips were sterilized by rinsing with 70% Ethanol and either dried at 70° C or rinsed with 96% Ethanol, to speed up the evaporation process. Figure 9 depicts two different final chip designs. The left one (2D-chip) had a single chamber volume of 28 μl and a chamber surface of 23.6 mm^2 , the right one (micromass-chip) 415 μl and 193.8 mm^2 . In order to increase the chamber volume in the micromass-chip, two glass channels were put on top of each other combined with another adhesive layer. Also incorporated in the micromass-chip design was a PDMS barrier with an inner diameter of 3 mm and an outer diameter of 5 mm to help micromass build up and immobilization. Assembly and loading of the micromass-chip intertwined as is described in section 3.3.

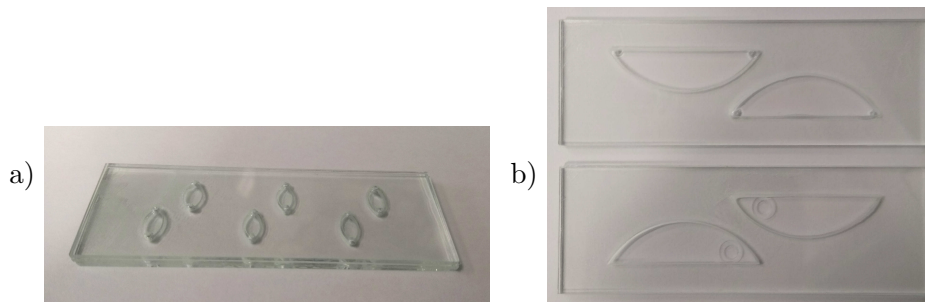


Figure 9: a) Finished 2D-chip. b) Semi-finished micromass-chip for experiment - parts are put together after chip loading.

3.3. Chip Loading

Surface coating of chambers (if used) was done by using S-Layer, a self-assembled anti-fouling coating preventing cell adhesion. Prior to coating, chambers were rinsed with 70 % Ethanol and stored for 24 hours in order for the Ethanol to evaporate. S-Layer was applied 6 to 24 hours before the actual loading process. Chips were put in a sterile

petri dish which was enclosed with Parafilm and stored at 4° C. Right before loading the S-Layer was removed with a pipette and the chamber rinsed once with filtered water. Afterwards the chip was ready to load. For experiments with cells in chips the growth medium was adjusted (chip-medium) by adding 1% Insulin-Transferrin-Selenium, 1% Vitamin C (L-Ascorbic Acid) at a concentration of 0.0316 mg per ml and 2% 4-(2hydroxyethyl)-1-piperazineethanesulfonic acid (HEPES).

Chips Based on Experiments with Mold Design

Using the mold chip production technique (section 3.2) first 2-dimensional experiments were set up with chips closed off with a glass slide after loading. Though these chips can be produced rapidly and offer compartmentalized loading (see figure 6b) the sealing process with glass caused the incorporation of air bubbles in the chamber. These bubbles created air-liquid-interfaces which could hinder cell movement, produce artifacts in measurement (e.g. microscopy or light scattering) and change the total volume (therefore the cell density) per chamber. To circumvent these disadvantages chip production was redesigned with the use of adhesive tape and loading ports (see section 3.2).

Chips for Experiments Based on 2-dimensional Biology

Cells were washed, trypsinated and centrifuged as described in section 3.1. By the use of a hemacytometer (Neubauer-Improved) cells were counted and the cell pellet resuspended (using chip-medium) to achieve desired cell density. After loading the top surface of the chips was swiped with a tissue and 70% Ethanol to clean and dry the surface. To avoid contaminations in the inlet and outlet ports the surface was closed off by the means of PCR foil (Adhesive PCR Seal).

Chips for Experiments Based on Pre-Grown Micromasses

Prior to chip loading micromasses were cultured in polyHEMA coated 12 well plates with 2 ml of chip-medium each. Culture time was set individually for each experiment. Transport of micromasses to chip was performed by using a 1 ml syringe (BD Plastipak, Becton Dickinson).

Chips for Experiments Based on Micromass Growth on Chip

As for 2-dimensional experiments cells were washed, trypsinated, counted, centrifuged and resuspended. Cells in chip-medium were mixed with matrigel in a ratio of 1:4 and stored on ice if not immediately used. Matrigel itself was thawed at 4° C for 30 minutes before usage. 15 μ l of the matrigel-cell-medium mixture was pipetted in the center of the PDMS barrier, see figure 10.

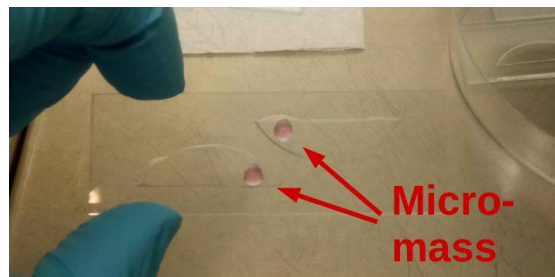


Figure 10: Matrigel-medium-cell-mixture in bottom side of micromass-chip.

Chip assembly was finished, the chip closed off with PCR foil and then put into an incubator at 37° C for 35 minutes in order for the matrigel to polymerize. After polymerization the PCR foil was removed, the chip loaded with chip-medium and once again closed off by PCR foil for contamination free storage in an incubator at 37° C.

3.4. Experiment Design

In this section details for individual experimental set-ups are described. Cells used in experiments were derived from multiple patients, but within one experiment only cells from a single patient were used, unless otherwise noted.

Characterization of Light Scatter System for 2-dimensional and 3-dimensional Cell Analysis

Within this set of experiments light scatter measurements were performed on a 2D-chip containing only chip-medium (without HEPES). The highest value of this blank sample analysis was then used for limit of detection calculation. A sample size of three was used for both OPD channels of the light scatter station for a single measurement.

Influence of Laser Power on Light Scattering In this experiment synoviocytes at various cell densities were seeded onto 2D-chips and used for light scatter measurements at different laser power after two hours of seeding. Medium used is chip-medium without HEPES. Cell densities used are 0, 2.5×10^5 , 1.0×10^6 and 3.0×10^6 cells per ml. Laser power values on chip used are 9.18, 39.8 and 82.2 μW . Sample size is three, but due to problems during chip loading one chamber of the medium control (0 cells / ml) contained air bubbles and was therefore excluded from the results.

Influence of Cell Density on Light Scattering This section describes 2- and 3-dimensional characterization experiments for different cell densities. Cells were seeded on the one hand in 2D-chips containing chip-medium and cell numbers of 0, 2.5×10^5 , 1.0×10^6 and 3.0×10^6 cells per ml. On the other hand cells were mixed with matrigel and loaded in micromass-chips as described in 3.3 with cell numbers of 0, 1.0×10^6 , 3.0×10^6 and 5.0×10^6 cells per ml. Cell densities per area and chamber in case of 2D-chips are depicted in table 4. Due to cell agglomeration, also described in sections 4.2, 2D-chips

with cell densities of $1.0 * 10^6$ cells per ml were discarded from the analysis. Sample size of 2D-chips was three. For micromass-chips, due to problems with chip loading sample size was one. These problems manifested themselves in a suction of the matrigel-medium-cell-mixture to chamber walls immediately after loading. Measurements were conducted on day 2 after seeding.

Table 4: Cell number for various cell densities on 2D-chips

Cell number per ml	Cell number per cm^2	Cell number per chamber
3 000 000	356 000	84000
1 000 000	119 000	28000
500 000	59 300	14000
250 000	29 700	7000
100 000	11 900	2800
50 000	5 930	1400

Impact of TNF- α on 2-dimensional Lining Layer Formation on Chip

2D-chips with and without S-layer coating were loaded with a concentration of $2.5 * 10^5$ cells per ml in chip-medium. Single light scatter measurements and microscope images were taken every day for a period of four days. Three samples were used for each of following conditions: FLS adherent, FLS non-adherent, FLS adherent with TNF- α , FLS non-adherent with TNF- α , chip-medium in non-coated chip, chip-medium in coated chip, chip-medium with TNF- α in non-coated chip and chip-medium with TNF- α in coated chip.

Every day after measurement medium exchange of about 10% of the chamber volume was performed for adherent cells to add fresh nutrients for the cells. In coated chips as cells were non-adherent no media exchange was performed.

Image analysis of non-adherent FLS with and without TNF- α was conducted by acquiring cell density, average cell diameter and area coverage for an area of 1.75 mm^2 for

each day of the experiment with ImageJ. Sample size for this analysis was set to one.

A live-dead assay was performed on day 4 as an endpoint analysis, as described in 3.1.

Analysis of Pre-Grown Micromasses

Micromasses were seeded with a cell density of $3.0 * 10^6$ cells per ml. Cultivation was conducted for a period of three to seven days in a polyHEMA-coated 12 well plate with 2 ml of chip-medium each. Starting on the third day four micromasses were daily transferred to the chips, composing of cylindrical holes in a PDMS layer on a glass slide. Transport was done using a 1 ml syringe (BD Plastipak, Becton Dickinson). A single light scatter measurement was performed and microscope images taken for each micromass which were discarded immediately afterwards. Only a single laser beam is used in this experiment as the used chip consists only of one chamber (see section 3.2).

Micromass Analysis in Self-Centering Spherical Cavities

Micromasses were seeded with a cell density of $3.0 * 10^6$ cells per ml and cultured for four days in a polyHEMA-coated 12 well plate. Cells from three different patients were each cultured in chip-medium, chip-medium containing 5 ng per ml Interferon- γ and chip-medium containing 10 ng per ml TNF- α . Sample size was set to four for each patient and condition. At the fourth day micromasses were transferred to the chips with semi-spherical cavities in a PDMS layer. Transport was done using a 1 ml syringe (BD Plastipak, Becton Dickinson). A single light scatter measurement was performed and microscope images taken for each micromass which were discarded immediately afterwards. Only a single laser beam is used in this experiment as the used chip consists only of one chamber (see section 3.2).

Impact of TNF- α on 3-dimensional Micromass Formation on Chip

Micromasses were seeded with a cell density of 3.0×10^6 cells per ml in S-layer coated micromass-chips. Three chips were filled with chip-medium and four with chip-medium containing 10ng per ml TNF- α . Each chip consisted of two chambers with a micromass each. Due to challenges in chip loading the sample size usable for micromass analysis was three in both conditions. Microscope images were taken daily prior to light scatter measurements. Medium exchange (150 μ l at day 1, 80 μ l at the following days) was performed daily with the respective chip-medium for each condition.

3.5. Light Scatter Station

The light scattering station (see figure 11) mainly consisted of three parts: 488 nm laser, measurement platform and signal analysis.

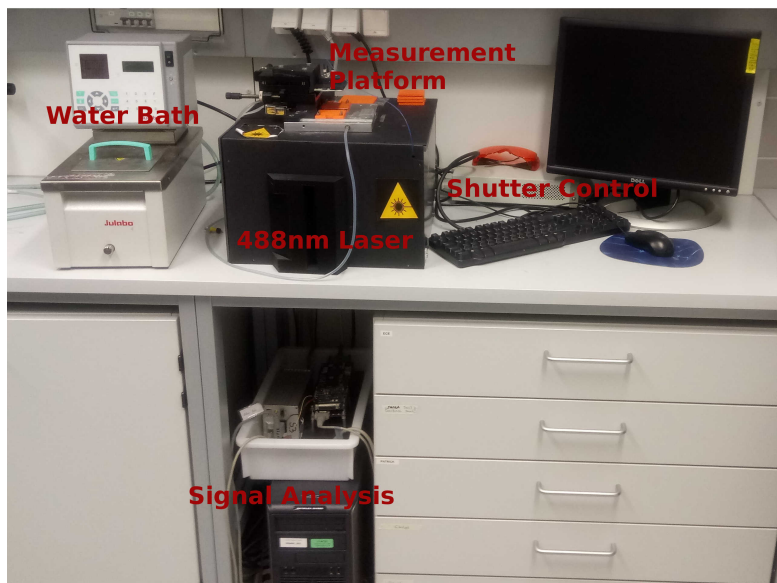


Figure 11: Light scatter station set-up

A sapphire laser created a 488 nm laser beam which was directed by the help of mirrors, beamsplitter and fiber coupler towards the measurement platform. There, the

beam first hit onto a microchip (including the biology of interest) and then a notch filter. Only scattered light with an angle greater than 20° to the incident light beam could pass the filter and was detected by an OPD. The remaining laser beam generated an electric signal in the form of a potential difference, which was displayed. Permanent illumination or the interval between illuminations could be set by a shutter. Laser power, shutter control and data storage were controlled by a LabView program. By the means of an x-y-table and a 3D printed mount for collimation the laser beam of the two used fiber couplers could be each directed onto an OPD (see figure12), named channel 1 and channel 2.

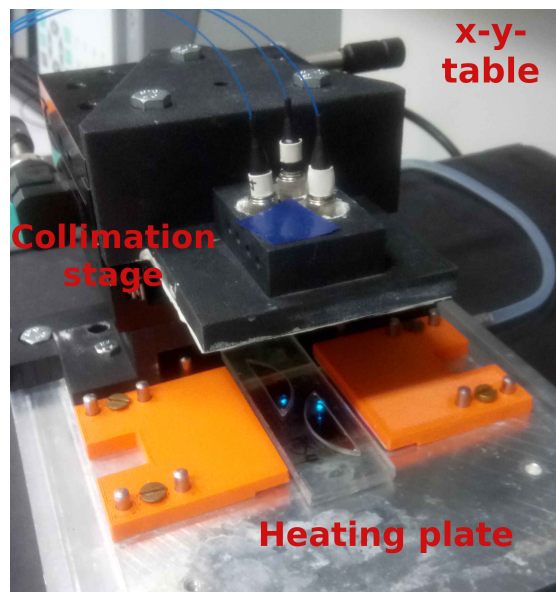


Figure 12: Light scatter stage close up

Laser power could be set between 7.5 mW and 82.5 mW. However due to equipment age, losses along the light path (see figure 13) and the used neutral density filter, the maximum output signal at the measurement platform was in the range of 7 to 85 μW . A handhold powermeter was used to determine and log the output laser power.

A water bath connected to the measurement platform enabled temperature control of

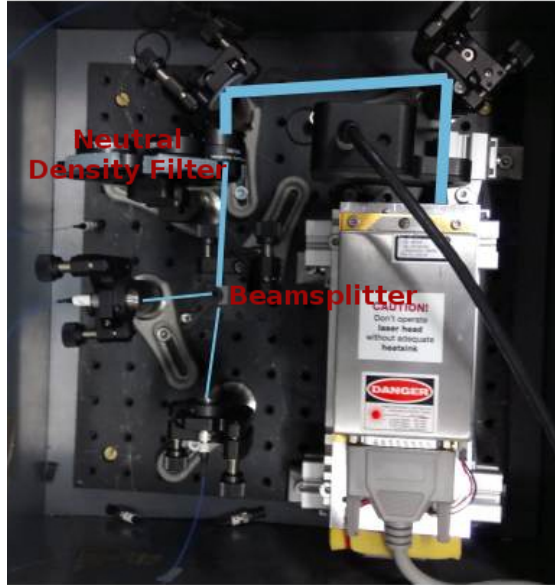


Figure 13: Light path from laser to fiber coupler

the chip. Setting bath temperature at 40.80°C resulted in the desired 37°C of the chip, which was derived by the help of a microscope slide with a Pt 1000 on top coupled to a multimeter.

3.6. Data Acquisition and Output

An already existing LabVIEW program (see figure 14) was used to read out and save the data points.

All experiments displayed were measured with the maximum laser power of about $83\ \mu\text{W}$. Single measurements were performed for about 10 seconds and data points acquired every 0.1 second. The output laser power of channel 2 was lower compared to channel 1, and therefore the OPD output signal of channel 1 was interpolated to mimic same laser power of both channels. A mean of the data was calculated and stored for plotting by a program written in Python 3.0 (see A).

Limit of detection was calculated as three times the noise amplitude of the random

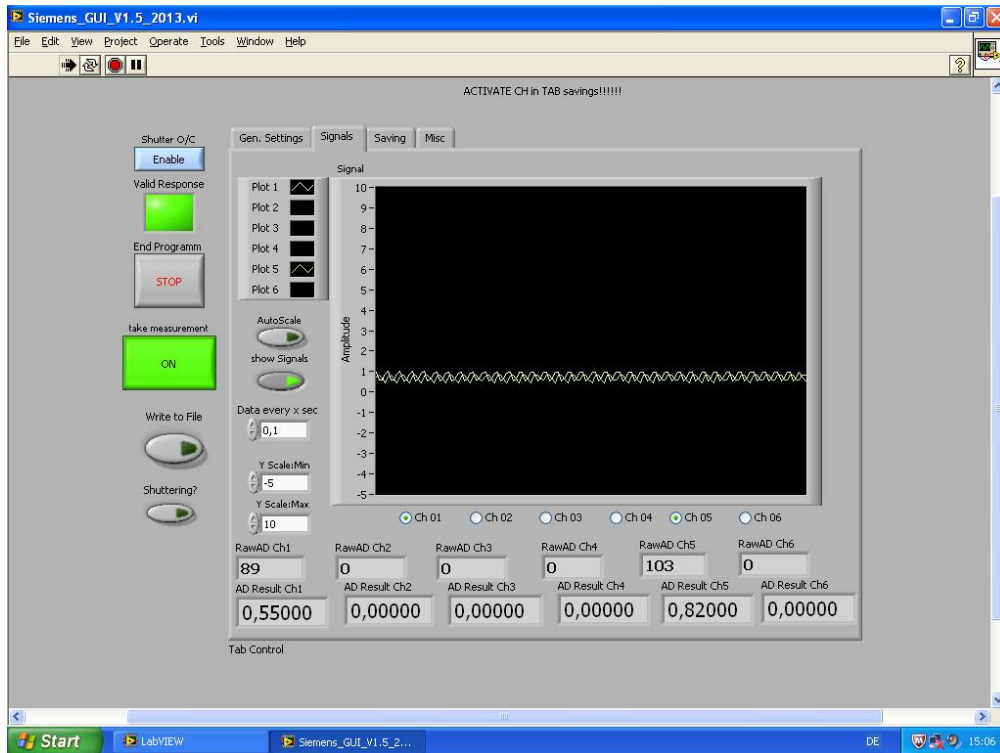


Figure 14: GUI of the LabVIEW program used to aquire data.

signal, as seen in equation 3.

$$LOD = 3 * Amplitude(Noise) \quad (3)$$

Figures were plotted by Libre Office Calc. Microscope images were taken with Olympus IX71 and fluorescence images with Olympus IX83. Figures and images were edited by Libre Office Draw and GIMP Image Editor.

4. Results and Discussion

4.1. Characterization of Light Scatter System for 2-dimensional and 3-dimensional Cell Analysis

Although light scattering of cell cultures has already been conducted with the measurement set-up previously, characterization of the light scatter system was performed for this study to analyze sensor sensitivity and linearity for 2- and 3-dimensional non-invasive analysis of synoviocyte cell cultures. Previously, normal human dermal fibroblasts (NHDF) and human umbilical vein endothelial cells (HUVEC) have been analyzed [50], however, never synovial fibroblasts, which differ from NHDF and HUVEC endothelial cells in phenotype as well as biologic function *in vivo*. Prior analysis of synoviocyte models for RA *in vitro*, important system parameters including blank medium values, limit of detection and laser power optimization as well as sensitivity towards increasing cell numbers were tested to identify optimal assay conditions.

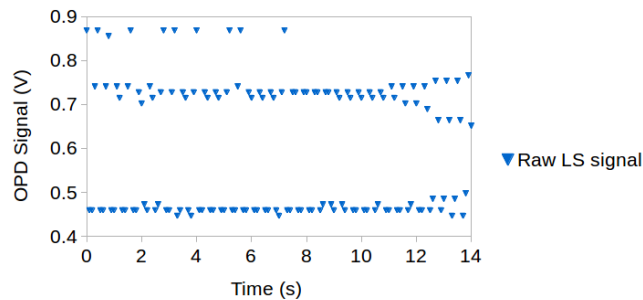


Figure 15: Light scatter measurement of blank sample (chip-medium in a 2D-chip) over time using channel 2 of light scatter station.

Prior to utilizing cells in experiments the limit of detection was determined for a blank sample. Figure 15 shows the raw output signal of the light scatter station for chip-medium on chip. The signal deviation of about ± 0.2 V is periodic, and therefore systemic. Applying of the mean value counteracts these periodic fluctuations.

Additional random signal changes of the maximum and minimum values in figure 15 account for the noise of the light scatter system. Figure 16a depicts the alteration of the average value at a given time. As described in section 3.6 the LOD is calculated as three times the span of this average signal, which is the noise. Both detection channels

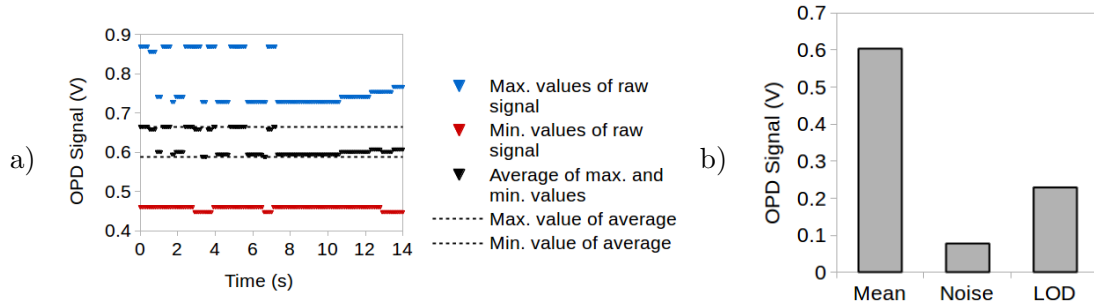


Figure 16: a) Maximum, minimum and average values of light scattering signal for a blank sample using channel 2 of light scatter station. b) Mean value, noise and LOD for a blank sample measurement using channel 2 of light scatter station.

of the scatter station displayed a similar noise behavior. The highest measured noise value is 0.077 V, corresponding to a limit of detection of 0.230 V. Whereas the related mean value of the blank sample caused a light scatter signal of 0.603 V, see figure 16b. Combined with the high range of detection spanning from 0 to 10 V, these facts underline the system's quality.

4.1.1. Influence of Laser Power on Light Scattering

Having the ability to use different values for input variables in measurement devices, increases their usability along with their detection range. In the next set of experiments different cell densities of still detached and round fibroblast-like synoviocytes are exposed to the full range of the system's laser power.

As can be seen in figure 17 there is a good correlation between the OPD output signal and the laser power used. Interestingly this holds true ranging from a blank sample to

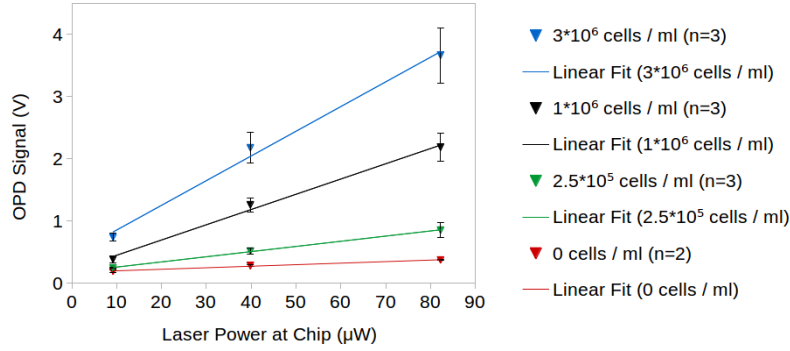


Figure 17: OPD output signal in regard to laser power at chip for different cell densities of fibroblast-like synoviocytes two hours after seeding on chip.

$3 * 10^6$ cells per milliliter and thus enables the investigation of different cell numbers on chip using light scattering for a broad range of cell densities applied initially as well as growing throughout the cell culture duration. It can also be seen that increased cell number yields an increased slope of the linear fit, in a range from 39.71 mV per μW laser power for $3 * 10^6$ cells per milliliter to 2.47 mV per μW for medium control, allowing distinction of cell density.

Furthermore this linear correlation is proof that light scatter signal can be intra- and extrapolated in the given range, which was done with channel 1 of the light scatter station, see section 3.6.

4.1.2. Influence of Cell Density on Light Scattering

Studies showed that formation of a thickened lining layer is a key feature of RA [13]. As fibroblast-like synoviocyte numbers in RA increase greatly *in vivo* due to several mechanism the determination of cell density with light scattering is of critical importance. In the next set of experiments synoviocytes in a 2-dimensional cell layer and a 3-dimensional micromass are compared. These conditions allow to mimic the lining layer and the environment *in vivo*, respectively. Overall cell density for 2-dimensional experiments was set lower, as only a cell layer is required, in comparison to a 3-dimensional

network in a micro-structure.

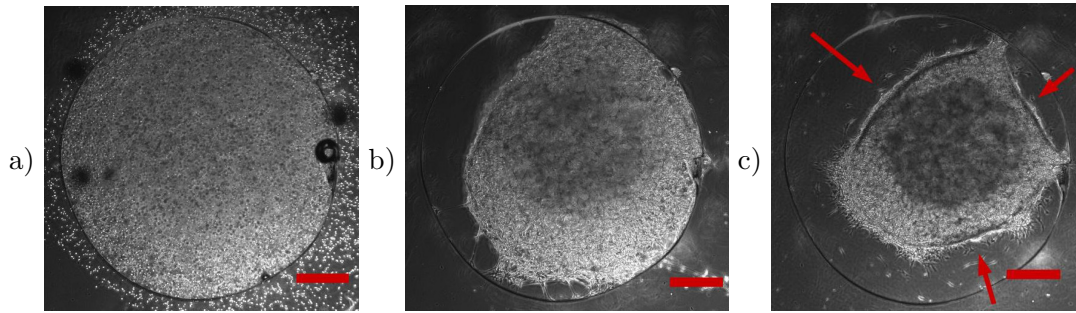


Figure 18: a),b),c) Formation of a micromass on a micromass-chip with a cell density of $3 * 10^6$ cells per milliliter on days 0, 1 and 2, respectively. Scale bar has a length of $500 \mu\text{m}$. Arrows in c) indicate lining layer formation.

Preceding the experiment observation of cells in both conditions are performed to establish a suitable measurement time point. 2-dimensional cell surface adhesion is visible after 24 hours. However, network and lining layer formation on the outer shell of the micromass takes longer. Figure 18 depicts cell morphology changes and beginning network formation at day 1 (figure 18b). Even so, onset of lining layer formation can be clearly seen to start at day 2 (figure 18c). Thus day 2 offers the ability to look into the influence of cell density in a 2-dimensional cell layer and a 3-dimensional micromass.

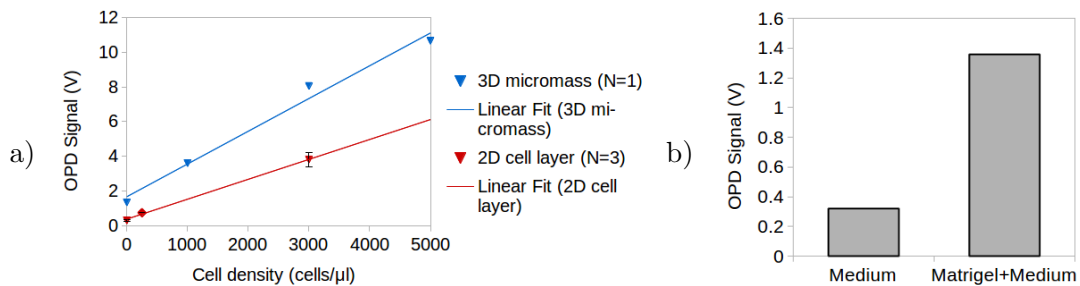


Figure 19: a) OPD signal of different concentrations of synoviocytes in 2-dimensional cell layer and 3-dimensional micromass 48 hours after seeding on chip. b) OPD signal of chip-medium in a 2D-chip and chip-medium and matrigel in a micromass-chip.

Next, the influence of increasing numbers of synoviocytes in a 2-dimensional monolayer and also embedded in Matrigel on the OPD signal was investigated. Linearity of cells in 2 and 3 dimensions in regard to the cell count can be seen in figure 19a. While cells with a density of $3.0 * 10^6$ cells per ml seeded in a 2-dimensional layer yield an OPD signal of 3.82 ± 0.42 V, same cell density in a 3-dimensional micromass correspond to a signal of 8.05 V. This is a clear indication that light scattering is not only sensitive to spherical cells, but is also able to distinguish cell density for elongated cells and even cells in a 3-dimensional network.

Interestingly the scattering signal of synoviocytes in a 3-dimensional structure has a greater y-axis offset and inclination. About 1 V is the difference of matrigel and medium to plain medium, leading to an four times increase in signal, see figure 19b. Matrigel consists to 30% of collagen IV. Gelation increases it's absorbance due to elevated turbidity of the protein network. This behavior was already reported by by Tsilibary et al [65].

Nevertheless the steeper increase of the scattering signal is not caused by the matrigel, but by the increasing number of cells illuminated in scattering.

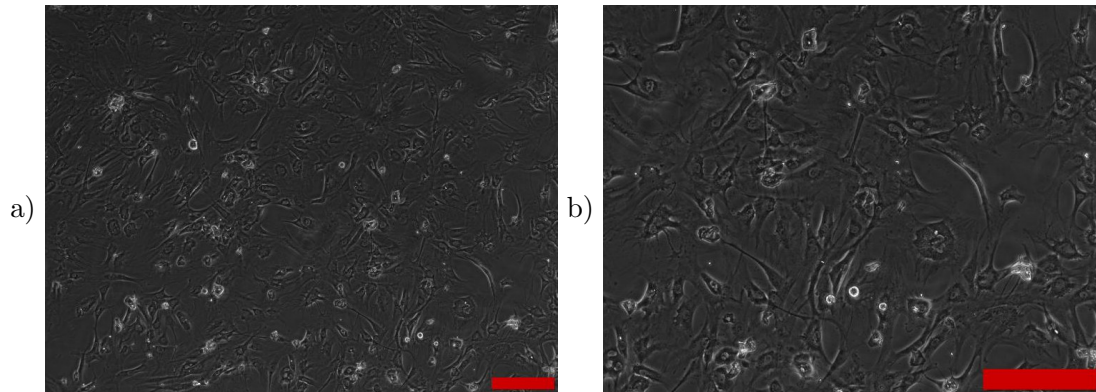


Figure 20: a),b) Fibroblast-like synoviocytes in a 2D-chip at a concentration of $2.5 * 10^5$ cells per ml. Scale bar has a length of $500 \mu\text{m}$ and $200 \mu\text{m}$, respectively.

Apart from a characterization measurement this experiment is also used for determi-

nation of suitable cell density for further 2-dimensional experiments. A cell count of $2.5 * 10^5$ cells per milliliter shows good coverage across the chip surface, yet no total confluence is reached (see figure 20 for comparison). Yielding a condition which allows a bottom up approach using a 2-dimensional monolayer for a synovial lining layer. Furthermore cell proliferation, a feature of vital importance in rheumatoid arthritis, is still possible.

To validate cell viability inside a 3-dimensional micromass, an endpoint live-dead assay was conducted at day 4. Figure 21 shows a very high percentage of viable synoviocytes, thus ruling out that cell necrosis affects outcome of later experiments over the course of four days.

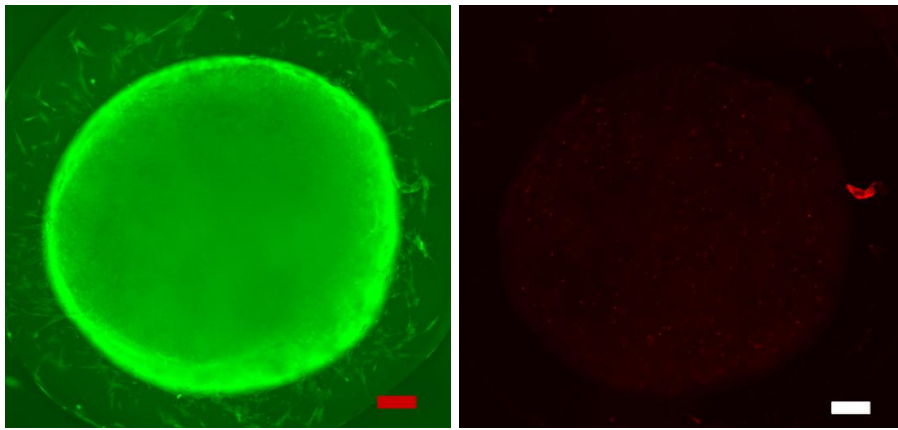


Figure 21: Fluorescence images of live (green) and dead (red) synoviocytes at day 4 of micromass culture obtained by using a Live/Dead Cytotoxicity assay based on Calcein and Ethidiumhomodimer. Cell count in the micromass was seeded at $5 * 10^6$ cells per milliliter. Scale bar has a length of $200 \mu\text{m}$.

4.2. Impact of $\text{TNF-}\alpha$ on 2-dimensional Lining Layer Formation on Chip

In the next set of experiments a bottom up approach was used to validate light scattering as a powerful non-invasive measurement tool for 2-dimensional experiments. Analysis of adherent and non-adherent cells becomes possible by chip surface coating with S-layer,

a self-assembled anti-fouling coating preventing cell adhesion. Introduction of TNF- α at a concentration of 10 ng per ml allows the simulation of an inflamed 2-dimensional lining layer.

Before starting the experiments, temperature of the microscope and light scattering stage were calibrated. As Watanabe et al presented cell growth dependency on culture temperature in time frame of hours [66]. Although in this set of experiments time outside of the incubator was limited to minutes at a time, controlled chip temperature of 37° C was desired. This way the impact of temperature fluctuations on the experiment could be ruled out.

The bottom up approach reduces complexity and enables investigation of one aspect at a time. First the impact of used medium on light scattering signal is analyzed. One major part of cell culture medium are proteins, which have been shown to be detectable by light scattering in the past [67].

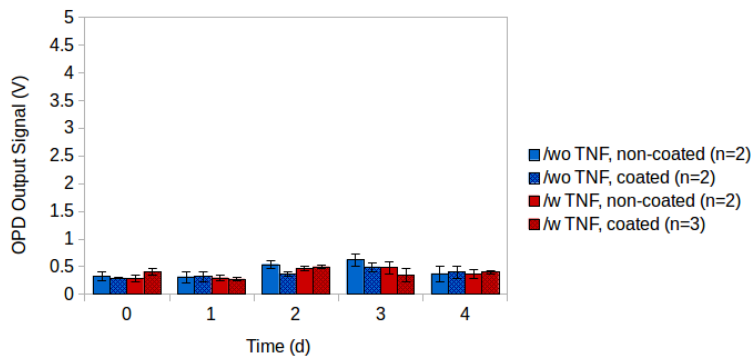


Figure 22: Light scatter measurement of chip-medium with and without TNF- α in non-coated and S-layer coated chips. TNF- α concentration is set at 10 ng per ml.

Overall the light scatter signal of chip-medium (see figure 22) is quite stable, ranging from 0.3 to 0.6 V. Signal fluctuations can be seen in all conditions. The height of these fluctuations combined with a rather high standard deviation in nearly all conditions and a limit of detection of the station of 0.23 V makes the impact of medium components

negligible. Cleanliness of optical elements and the application of PCR foil are most likely responsible for increase in signal deviations.

Morphology changes are vital for cell adhesion and network formation of adherent cells. As the lining layer formation in the inflamed synovium represents such a network, investigation of morphology is of great interest. Figures 23a,b depict schematics of a round cell with nucleus and its transformation to an elongated one. Respective microscope images 2 h and 24 h after seeding are above the schematics. Light scatter signal

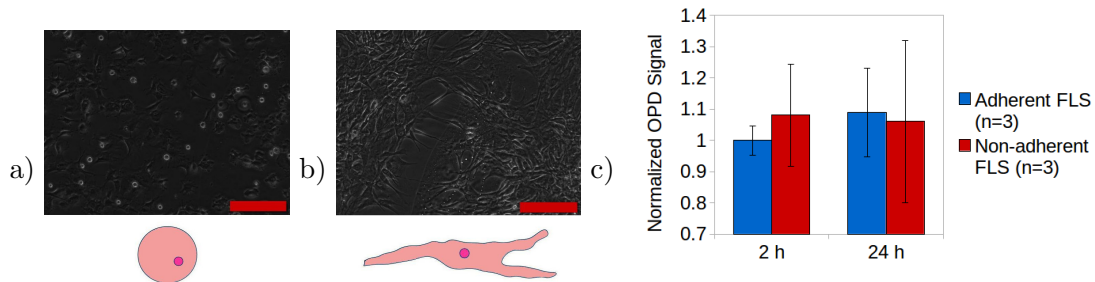


Figure 23: a) Schematic of a round cell and b) an elongated cell with nucleus with corresponding microscope images above. Chip surface was not altered by surface coatings. Scale bar has a length of 200 μm . c) Light scatter signal of adherent (non-coated) and non-adherent (S-layer coated) synoviocytes normalized to the signal of adherent synoviocytes at 2 h after seeding. Measurements were taken 2 h and 24 h after cell seeding.

in figure 23c clearly shows the effects of cell adhesion and morphological changes. While normalized signal of adherent cells increases by 8,1% due to network formation and larger occupied surface area, the signal of non-adherent round cells slightly decreases. This offers not only an extremely fast non-invasive method for detection of morphological changes, but also enables the study of 2-dimensional lining layer formation.

In the next step a 2-dimensional lining layer is studied along with its changes under the influence of $\text{TNF-}\alpha$. $\text{TNF-}\alpha$ could induce RA in mice [27] and is here used to create an inflamed status. Figure 24a shows the light scatter signal of adherent fibroblast-like synoviocytes with and without $\text{TNF-}\alpha$. An initial signal increase in both, healthy

and diseased, cases can be seen and correlates to a network formation within the cell population. Starting on day 3 the light scatter signal of synoviocytes without TNF- α decreases reaching a value below the starting value at day 4, whereas the one of cells with TNF- α keeps increasing accumulating to a 2.4 fold increase at day 4 compared to day 0. Comparing the signal with microscope images in figure 24b,c it can be seen that cells without the cytokine (b) begin to agglomerate and cluster at day 2. These spheroid shaped agglomerates lead to a massive overall reduction of chip surface coverage leading to a decline in scatter signal. As the agglomerates are not necessarily in the laser beam area (chip surface of 23.6 mm², laser beam 4.5 mm²), their signal contribution cannot be guaranteed. One probable cause of the adhesion loss are the surface conditions of the untreated microscope glass slides. If one compares these smooth surfaces to cell culture treated ones, it can be seen that several techniques are used by manufacturers to enable better cell growth.

Even as interesting as the adhesion loss of cells without TNF- α is the continued adhesion of those stimulated with that represent the RA phenotype. These yield a signal increase from 0.73 +/- 0.07 V at day 0 to 1.72 +/- 0.46 V at day 4. Microscope images in figure 24c show network formation and tightening, which in combination with TNF- α enhanced cell proliferation, yield the ongoing signal increase in figure 24a. Stimulation of synoviocyte activation by TNF- α was reported to enable the cells to produce various compounds such as ICAM-1, VCAM-1 and integrins [68],[13], see section 1. This increased amount of adhesion molecules leads to the observed behavior.

In order to distinguish the impact of TNF- α stimulation on morphology of fibroblast-like synoviocytes, the next set of experiments with non-adherent cells in chips coated with S-layer were conducted. As the synovium sublining consists of a loose connective tissue with various cells, this experiment design also acts as a first attempt to mimic and analyze its structure with light scattering. Image analysis indicated that light scatter signal for similar cell size is dependent on the area coverage, see figure 25a-d. At day

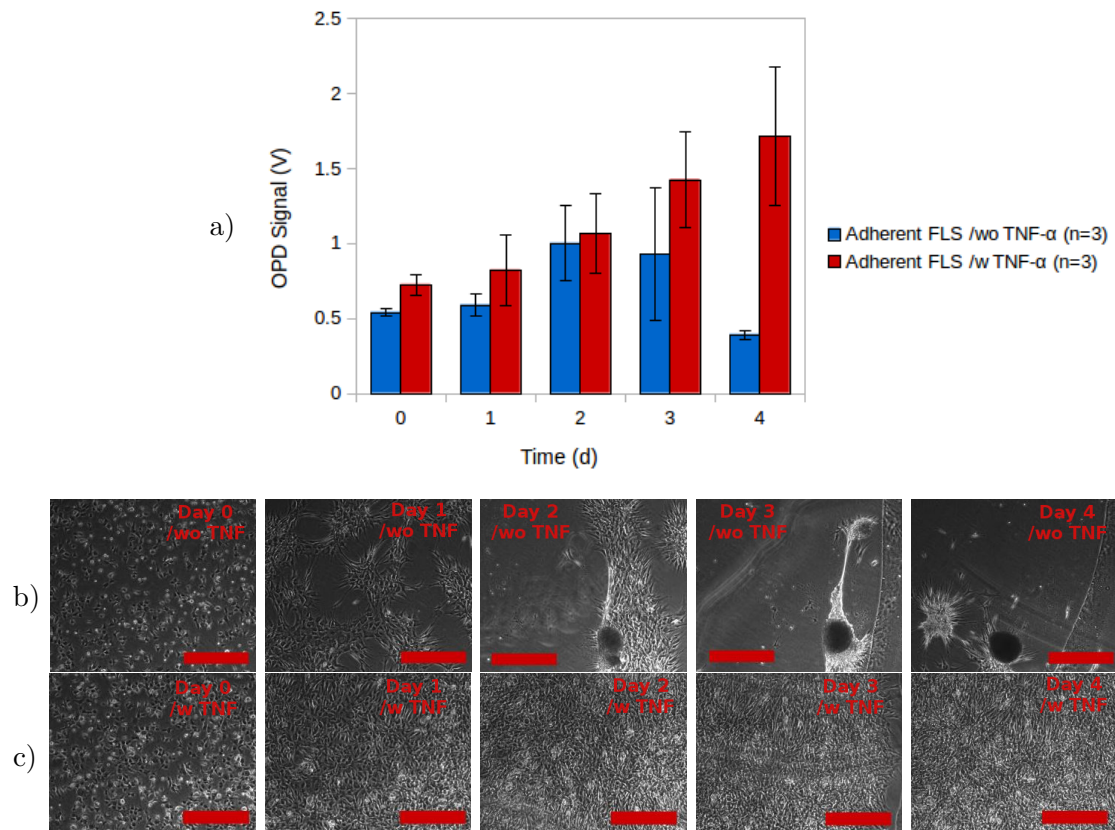


Figure 24: a) Light scatter measurement of adherent fibroblast-like synoviocytes with and without $\text{TNF-}\alpha$ on chip over four days. $\text{TNF-}\alpha$ concentration was set at 10 ng per ml. b) Corresponding microscope images of synoviocytes without $\text{TNF-}\alpha$ and c) with $\text{TNF-}\alpha$. Scale bar has a length of 500 μm .

0 a sample chip with $\text{TNF-}\alpha$ showed increased area coverage and slightly increased average cell diameter and density compared to the chip without $\text{TNF-}\alpha$. As expected this also results in higher light scattering signal. Interestingly a drop in area coverage in both conditions did not yield a decrease of scatter signal, but an increase. Therefore the formation of cell agglomerates, which is represented by the increase in average cell diameter and reduction of the cell count, is responsible for the enhanced light scatter signal. Hence less large cell agglomerates give rise to more light scatter signal than many single cells in this size regime. However the area coverage is still decisive if the other

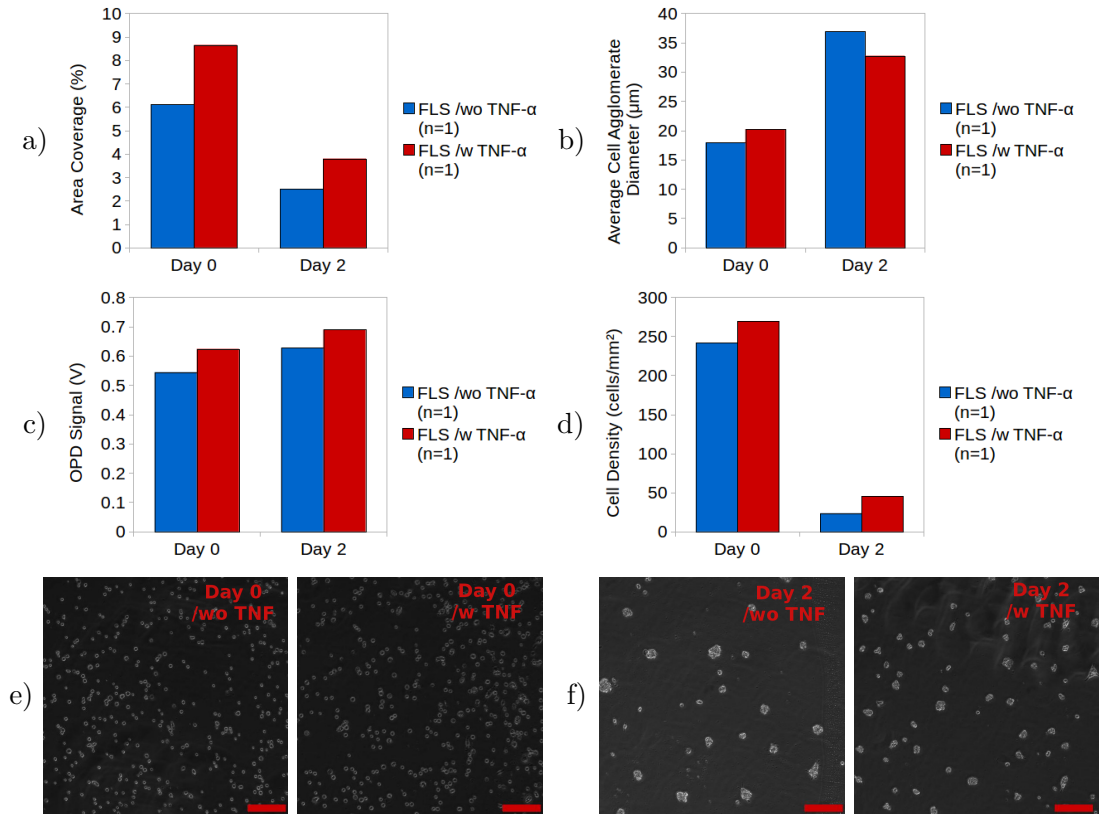


Figure 25: a) Area coverage, b) average cell agglomerate diameter, c) light scatter signal and d) cell density of non-adherent synoviocytes in S-layer coated chips. Graphs show analysis of one microscope image for one sample with chip-medium and one sample with chip-medium containing 10 ng per ml TNF- α at day 0 and day 2 after seeding. Microscope images are depicted in e) at day 0 and f) at day 2. Scale bar has a length of 200 μm .

parameters are similar as the sample with TNF- α shows higher scatter signal and area coverage, but less average agglomerate diameter.

In figures 25e,f microscope images of the synoviocytes at day 0 and 2 can be seen and show the same behavior as the image analysis. Formation of less but larger cell agglomerates is distinctive visible at day 2 in cells without TNF- α .

The significance of TNF- α in this experiment represented itself by the increased cell density and reduced agglomerate diameter at day 2. Interestingly, also non-adherent

fibroblast-like synoviocytes expressed different behavior when exposed to the cytokine, yet exact mechanism remain unclear.

Comparing light scatter signals of adherent and non-adherent synoviocytes with and without TNF- α , one can clearly see the impact of area coverage on the signal, see figure 26. Adherent cells with TNF- α exhibit the largest surface area and also the highest scatter signal. Adherent synoviocytes without TNF- α which form tight agglomerates from day 2 onward drop in scatter signal to a value of 0.39 ± 0.03 V at day 4 even below the non-adherent cells. This is due to the fact that all cells in adherent chips without TNF- α are packed in a few agglomerates. If these agglomerates are not illuminated by the laser, all the contained cells are lost to the scatter signal.

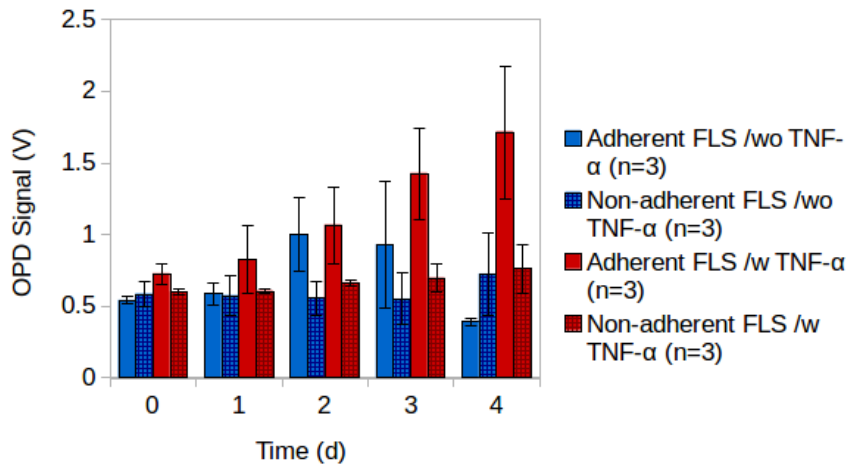


Figure 26: Light scatter measurement of adherent and non-adherent fibroblast-like synoviocytes with and without TNF- α over four days. TNF- α concentration was set at 10 ng per ml.

Finally, a live-dead assay was conducted and validated good cell viability at day 4 after seeding, see figure 27. In the case of dead non-adherent cells it cannot be ruled out that these are a product of anoikis, which is apoptosis after cell-matrix-adhesion loss [69].

In the left panels of figure 27a synoviocytes without TNF- α in non-coated chips formed

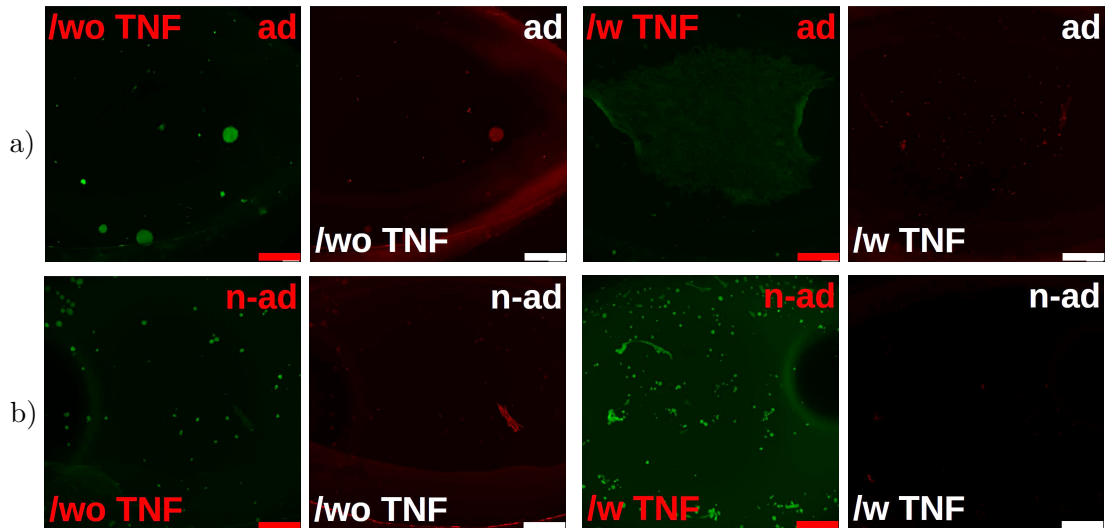


Figure 27: Live(green)-dead(red)-staining of a) adherent and b) non-adherent fibroblast-like synoviocytes with and without TNF- α at day 4 after seeding on chip. TNF- α concentration was set at 10 ng per ml. Scale bar has a length of 500 μm .

larger spherical structures than those with S-layer coating in part b. However, these coated chips without TNF- α show the same size regime of cell-agglomerates as coated chips with TNF- α (depicted in 27b). Due to the non-adherent state of synoviocytes in coated chips and in non-coated chips without TNF- α , cell-agglomerate number has been reduced by the live dead assay for these conditions. Combined with formation of 3-dimensional structures it is obvious that the area coverage of these conditions is diminished compared to adherent synoviocytes with TNF- α , see right panels of figure 27a.

4.3. Measurements of 3-dimensional Micromasses

Analysis of Pre-Grown Micromasses For initial experiments on 3-dimensional biology a top down approach was chosen. This was supported by the reports from Kiener et al. These had shown the ability of synoviocytes to form sphere-shaped micromasses with a lining layer when cultivated in matrigel and medium [30]. Various compounds activate

and influence synoviocyte behavior *in vivo* and therefore have an impact on the lining layer. Cytokines, such as TNF- α and Interferon- γ , are one group of these compounds.

Prior to investigating the influence of cytokines on the micromass development, age differences of micromasses were compared. Figure 28 shows light scatter signal and microscope images of micromasses with age ranging from three to seven days after seeding. Four different micromasses were measured each day. A difference in micromass diameter and structure resulted in micromass wall attachment and micromass folding, which in turn was followed by different heights of the micromasses on chip. Incorporation of air bubbles under the tissue can also be seen, e.g. day 3 micromass #4, increasing the height difference further. One look at the output signal suffices to indicate that the micromasses and their light scatter signal cannot be compared to each other due to their height and structural deviation caused by the loading process. For instance micromass #2 on day 5 has a signal increase of 3 V compared to the next highest micromass. When investigating the corresponding microscope image, it can be seen that the micromass folded and attached itself to a chamber wall.

However, this experiment still yielded valuable information. Micromasses as Kiener et al used them were growing three weeks in a well plate before analysis [30]. Here it can be seen that already three days after seeding the micromass structure was visible and stable enough for the whole micromass to be pipetted onto a chip, leading to decreased time and consumable consumption for further experiments.

Micromass Analysis in Self-Centering Spherical Cavities Implementing a new chip design allows circumventing challenges in chip loading. Based on the gravitational pull of the earth, micromasses are self centering and their analysis therefore independent of the loading technique.

Micromasses built of cells derived from different patients show quite a varied behavior

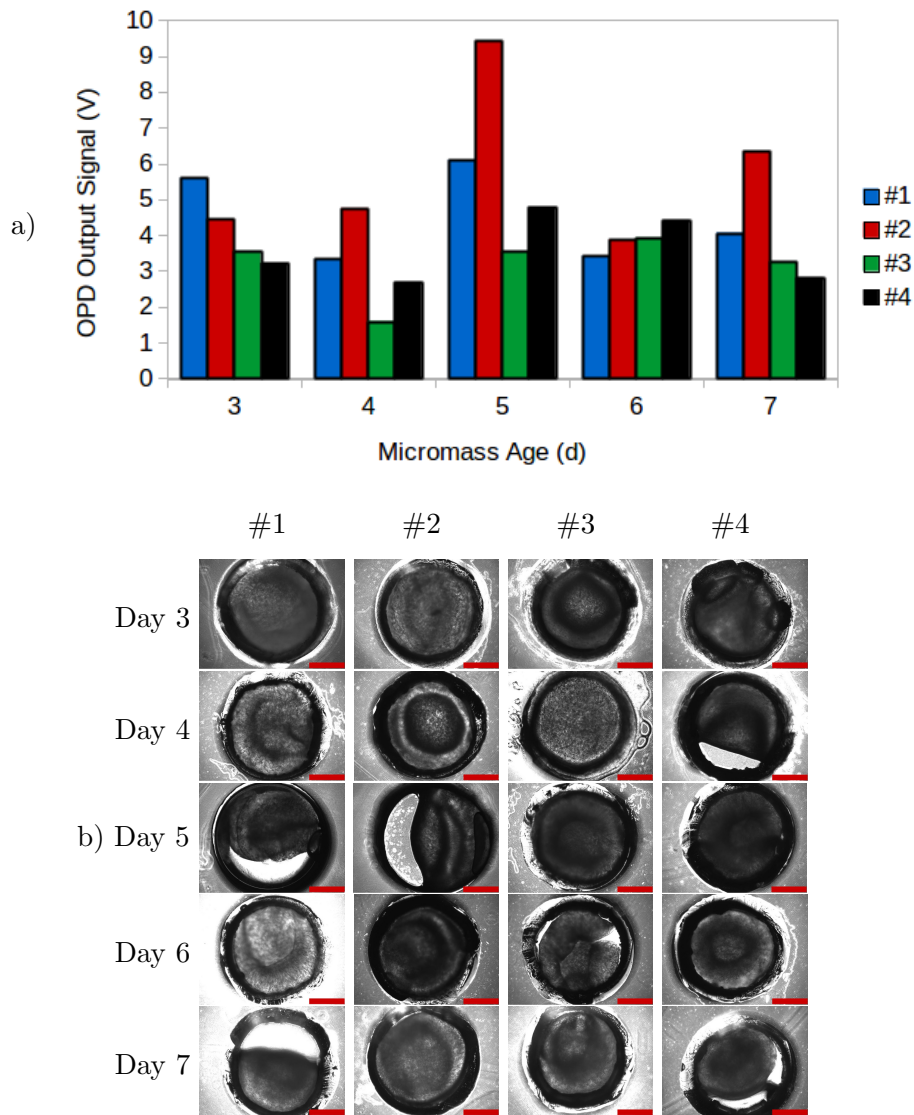


Figure 28: a) Light scatter measurement and b) microscope images of four different micromasses per day with increasing micromass age for a period of five days. Micromasses were cultivated in 12 well plates containing chip-medium. Scale bar has a length of 1 mm.

as seen in figure 29. Patient patient variation in RA was shown in studies by different responses to TNF- α blockers [70].

Interestingly also signal deviations appear in micromasses from the same patient and

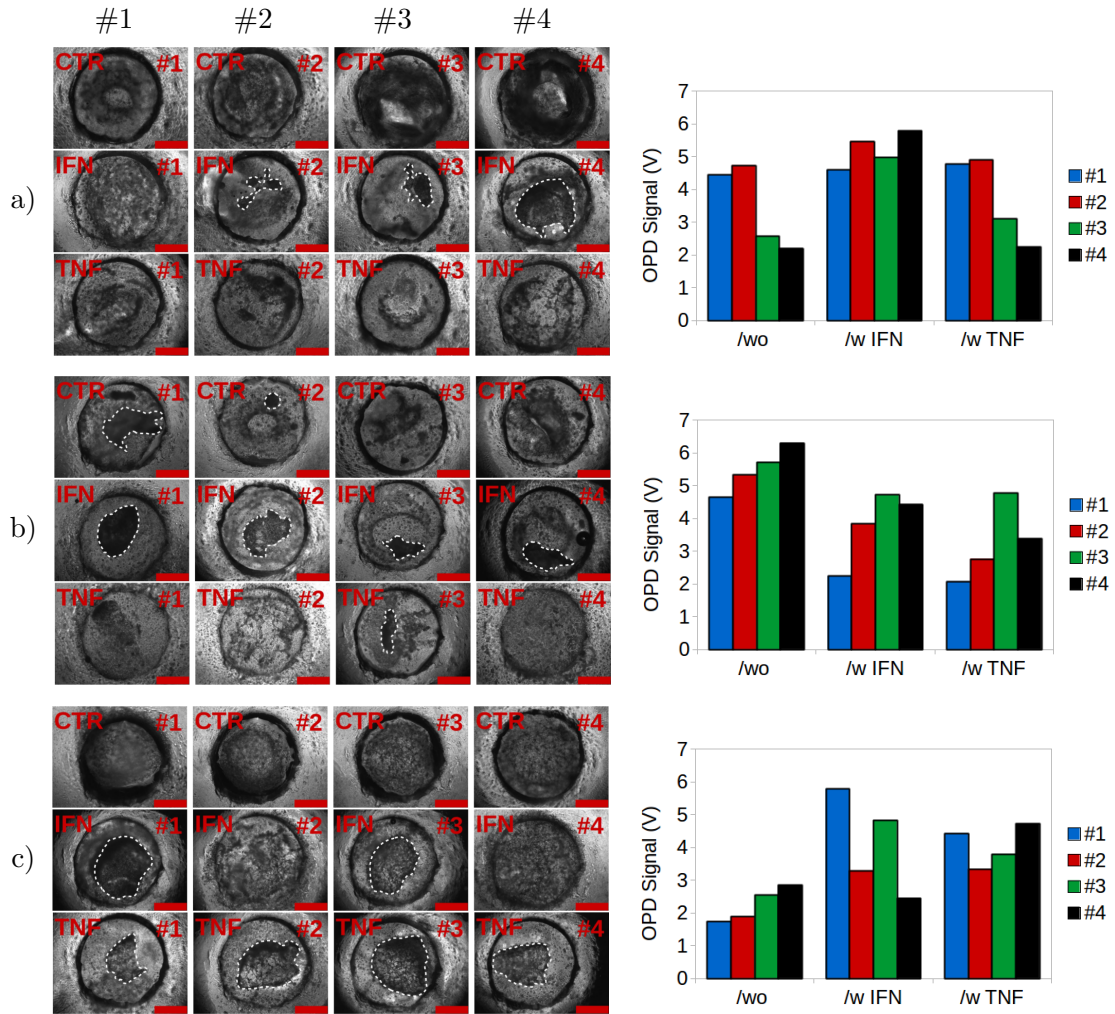


Figure 29: Microscope images and light scatter measurements derived from three (a,b,c) different patients. Twelve micromasses per patient were cultivated for four days in a 12 well plate - four with chip-medium(control), four with chip-medium containing 5 ng per ml Interferon- γ and four with chip-medium containing 10 ng per ml TNF- α . White dotted lines indicate secondary structures in micromasses. Scale bar has a length of 500 μm .

with the same culture medium. For instance two micromasses treated with Interferon- γ in figure 29c (#1 and #3) show a well defined secondary structure along with a high light scatter signal in the range of 5 to 6 V. The remaining two micromasses (#2 and #4) show a network inside the micromass but not a distinctive secondary structure. When

investigating their scatter signal, a clear drop, to about 3 V, can be seen in comparison to the first two.

Overall it can be seen that micromasses showing secondary structures (indicated in figure 29 by white dotted lines) produce higher scatter signal than structure-wise homogeneous micromasses. Thus there may be a variation in which way micromasses derived from different patients react on various cytokines. However, the light scatter signal reflects the structural information inside the micromass, and even can reflect different responses based on patient to patient variation in a precise manner.

4.3.1. Impact of TNF- α on 3-dimensional Micromass Formation on Chip

Above experiments support micromass structural and network formation up to day 3 after seeding. In this set of measurements micromasses are grown on chip. Influence of TNF- α on micromass formation in this crucial time frame can be analyzed continuously by non-invasive light scattering. Chip chamber surfaces are coated with S-layer prohibiting cell surface attachment thus enabling micromass formation.

At the start of the experiment chips are loaded as described in section 3.3. Due to prior challenges of matrigel and S-layer an increased amount of S-layer protein was used (1:5 instead of 1:10, corresponding to 200 μ l per ml) to enhance the surface coating.

Although these precautions were installed chip loading succeeded in only six of fourteen cases. Figure 30a depicts microscope images of the micro structure in one of the discarded chips. Matrigel wall attachment at the time of loading leads to a permanent one causing reduced cell number in the detection zone and different structural behavior. This phenomenon was caused by the hydrophilicity of the surface at the time of loading due to the coating. Figure 30b confirms these deviations in micromass formation by plotting the light scatter signal of the micro structure seen in figure 30a normalized to the mean of intact micromasses used in experiment analysis. Over the course of four days the normalized signal declines, resulting in a 23% drop, and emphasizes the need

to discard not properly loaded chips from the experiment.

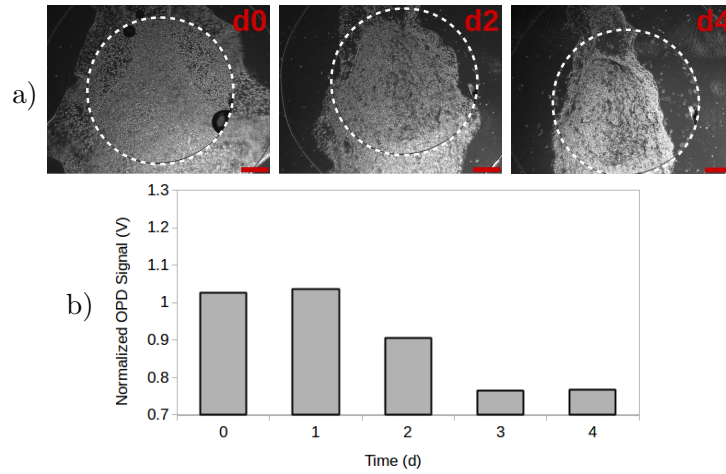


Figure 30: a) Microscope images and b) light scatter measurements of one sample chip discarded from the analysis. OPD signal is normalized to the mean of chips used in analysis with same treatment. White dotted lines emphasize the inner ring of the PDMS barrier on the chip. Scale bar has a length of 500 μm .

Six micromasses, three with chip-medium and three with chip-medium containing TNF- α were analyzed by light scattering over the course of four days. Overall analysis and microscope images over time of one micromass per condition are displayed in figure 31.

Figure 31a shows a signal rise for both experimental conditions, which are synovial micromasses cultivated in the presence and absence of TNF- α whereas microscope images are depicted in figures 31b,c for micromasses without and with TNF- α respectively. In the right panels of these images the micromass position inside the white dotted lines, which represent the inner ring of the PDMS barrier with an diameter of 3 mm, can be seen. This underlines the ability of site stable on-chip micromass growth with help of a PDMS barrier. Interestingly starting from day 2 light scatter signal of micromasses with TNF- α yields a greater signal increase compared to micromasses without. At day 3 and 4 the signal deviation is significantly higher with $*p \leq 0.05$ on day 3 and $**p \leq 0.01$

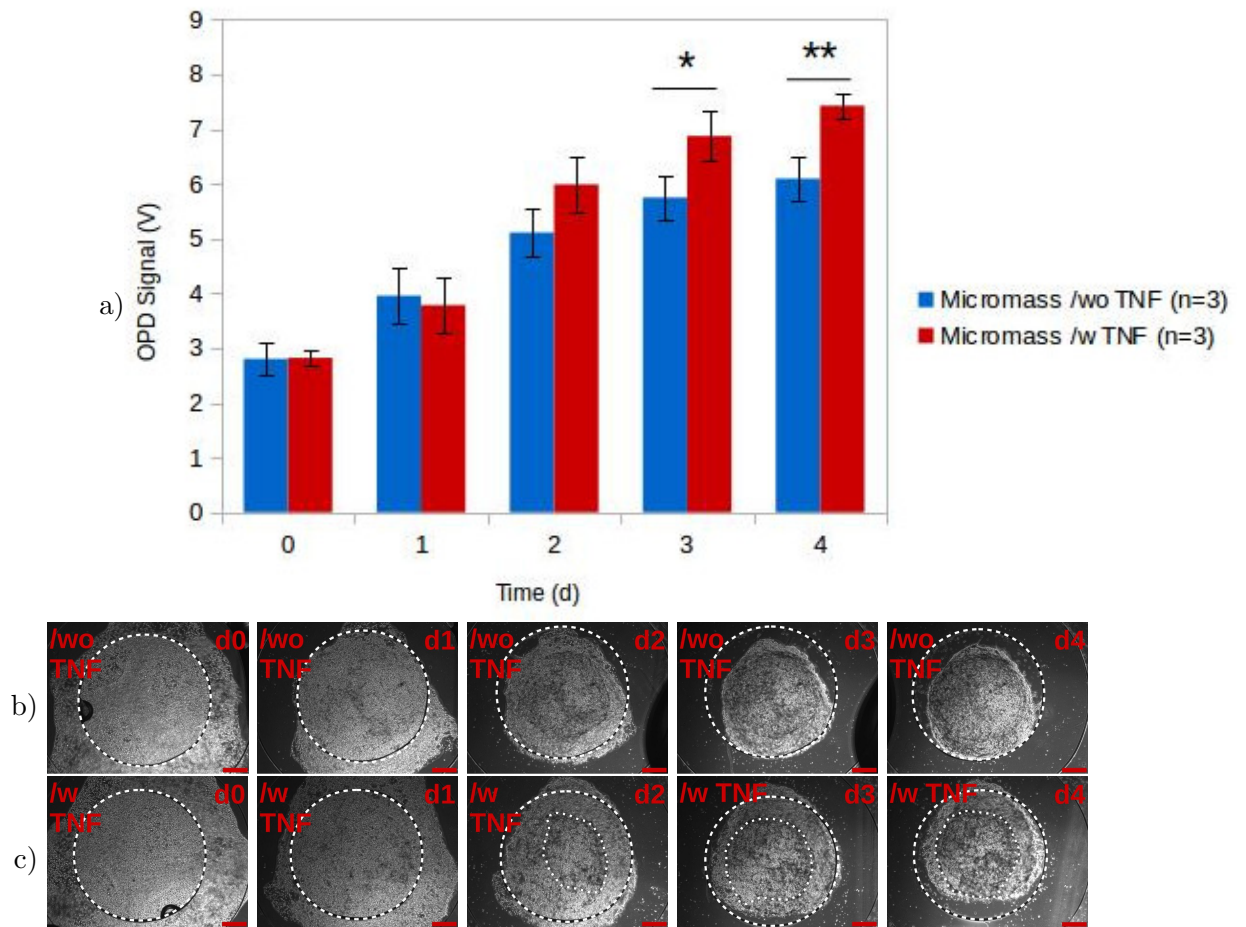


Figure 31: a) Light scatter measurement and microscope images of b) non-treated micromasses as well as c) micromasses stimulated with 10 ng per ml TNF- α cultured on chip over the course of four days. Inner white dotted lines indicate secondary structures within the micromass. The outer ring of white dotted lines emphasizes the PDMS barrier on the chip. Scale bar has a length of 500 μm . * $p \leq 0.05$, ** $p \leq 0.01$.

on day 4. At day 4 the light scatter signal of micromasses with TNF- α is 21.86% higher than for micromasses without. Cause for this signal increase are more dense secondary structures inside the micromasses with TNF- α , which build up is supported by the increased amount of adhesion molecules, a product of fibroblast-like synoviocytes. These secondary structures can be seen in figure 31c highlighted by the inner white dotted

lines. Micromasses without TNF- α lack these structures as depicted in figure 31b. The outer ring of white dotted lines emphasizes the PDMS barrier on the chip. A second contribution to the intensity of scattered light are synoviocyte products. As TNF- α has been reported to enhance fibroblast-like synoviocyte activation and therefore leads to a higher number of their products, including cytokines, cell adhesion molecules and growth factors [14].

An endpoint live-dead assay was performed and confirmed good cell viability. Interestingly it appears there is an accumulation of dead cells on the outside of the micromass (see figure 32), where cells are in direct contact with the chip-medium and therefore nutrients.

If dead synoviocytes were transported out of the micromass or the increase in proliferation due to TNF- α stimulation led to an overall increase in waste products, including dead cells, could not be verified.

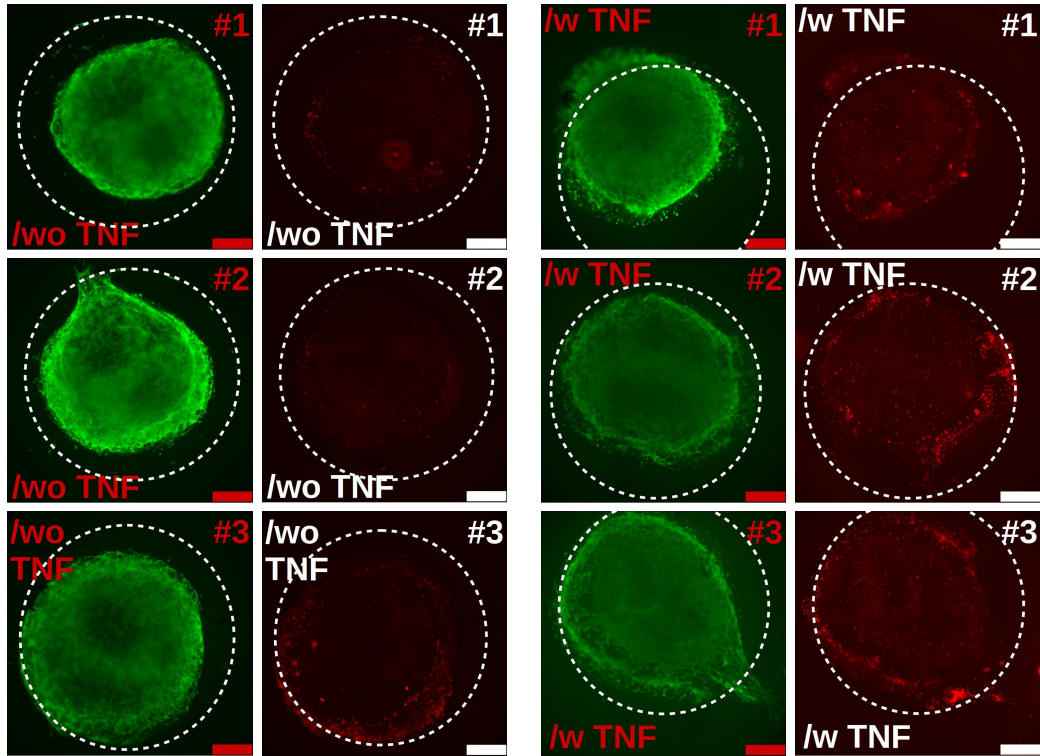


Figure 32: Fluorescence images of the micromasses used for data analysis on day 4 as an endpoint live(green)-dead(red) assay. Micromasses in the left panels were cultivated in chip-medium, those in the right panels in chip-medium containing 10 ng per ml TNF- α . White dotted lines emphasize the inner ring of the PDMS barrier on the chip. Scale bar has a length of 500 μm .

5. Conclusion

Light scattering has been shown to be a versatile tool for manifold applications in the past ranging from protein analysis in the μm range [67] towards whole finger joint measurements in RA patients [71]. In this thesis the gap between micro and macro was closed. In a novel technique light scattering was employed for non-invasive observation of tissue dynamics in RA, such as network formation or response to stimulants. A large linear range and application in analysis of 2- as well as 3-dimensional structures are cornerstones of this technique. Though cells derived from different patients could react differently, light scattering displayed reliable results by reflecting tissue structures in corresponding microscope images. Personalized medicine or one-person trials are slogans increasingly seen in literature and also media. Effective treatments of the top ten drugs with highest market value in the United States do only occur in 4-25% of patients [72]. Therefore the need of unhampered screening methods is all the more important. Responses of micromasses to treatments were shown within a time frame of three days, which is incredibly fast. If comparing this on-chip culture to past experiments by Kiener et al with micromasses cultured in well plates for a period of three weeks [10],[30], this is a vast improvement in time, therefore highly suited for more transient cellular processes that take place over hours and days, but not weeks.

In general, microfluidic and organ-on-a-chip microarrays have been reported to be an auspicious screening tool for biomedical applications [73]. Reduced amounts of reagents lead to a cut in costs and therefore may pave the way for application in personalized medicine. The technique developed in the frame of this thesis coupled with lab-on-a-chip micro fabrication can easily be adopted to suit other biological questions, making it a versatile and powerful tool for biomedical research.

References

- [1] Lisa M Coussens and Zena Werb. Inflammation and cancer. *Nature*, 420(6917):860, 2002.
- [2] Gökhan S Hotamisligil. Inflammation and metabolic disorders. *Nature*, 444(7121):860, 2006.
- [3] Gary S Firestein. Evolving concepts of rheumatoid arthritis. *Nature*, 423(6937):356, 2003.
- [4] Steffen Gay, Renate E Gay, and William J Koopman. Molecular and cellular mechanisms of joint destruction in rheumatoid arthritis: two cellular mechanisms explain joint destruction? *Annals of the rheumatic diseases*, 52(Suppl 1):S39, 1993.
- [5] Susan E Sweeney and Gary S Firestein. Rheumatoid arthritis: regulation of synovial inflammation. *The international journal of biochemistry & cell biology*, 36(3):372–378, 2004.
- [6] K Aho, M Koskenvuo, J Tuominen, and J Kaprio. Occurrence of rheumatoid arthritis in a nationwide series of twins. *The Journal of rheumatology*, 13(5):899–902, 1986.
- [7] AJ Silman, AJ MacGregor, W Thomson, S Holligan, D Carthy, A Farhan, and WER Ollier. Twin concordance rates for rheumatoid arthritis: results from a nationwide study. *Rheumatology*, 32(10):903–907, 1993.
- [8] Ernest HS Choy and Gabriel S Panayi. Cytokine pathways and joint inflammation in rheumatoid arthritis. *New England Journal of Medicine*, 344(12):907–916, 2001.
- [9] Chinh N Tran, Steven K Lundy, Peter T White, Judith L Endres, Christopher D Motyl, Raj Gupta, Cailin M Wilke, Eric A Shelden, Kevin C Chung, Andrew G

- Urquhart, et al. Molecular interactions between t cells and fibroblast-like synoviocytes: role of membrane tumor necrosis factor- α on cytokine-activated t cells. *The American journal of pathology*, 171(5):1588–1598, 2007.
- [10] David M Lee, Hans P Kiener, Sandeep K Agarwal, Erika H Noss, Gerald FM Watts, Osamu Chisaka, Masatoshi Takeichi, and Michael B Brenner. Cadherin-11 in synovial lining formation and pathology in arthritis. *Science*, 315(5814):1006–1010, 2007.
- [11] Sook Kyung Chang, Zhizhan Gu, and Michael B Brenner. Fibroblast-like synoviocytes in inflammatory arthritis pathology: the emerging role of cadherin-11. *Immunological reviews*, 233(1):256–266, 2010.
- [12] Adam Mor, Steven B Abramson, and Michael H Pillinger. The fibroblast-like synovial cell in rheumatoid arthritis: a key player in inflammation and joint destruction. *Clinical immunology*, 115(2):118–128, 2005.
- [13] Beatrix Bartok and Gary S Firestein. Fibroblast-like synoviocytes: key effector cells in rheumatoid arthritis. *Immunological reviews*, 233(1):233–255, 2010.
- [14] Erika H Noss and Michael B Brenner. The role and therapeutic implications of fibroblast-like synoviocytes in inflammation and cartilage erosion in rheumatoid arthritis. *Immunological reviews*, 223(1):252–270, 2008.
- [15] Paul P Tak, Nathan J Zvaifler, Douglas R Green, and Gary S Firestein. Rheumatoid arthritis and p53: how oxidative stress might alter the course of inflammatory diseases. *Immunology today*, 21(2):78–82, 2000.
- [16] Xiangli Li and Sergei S Makarov. An essential role of nf- κ b in the tumor-like phenotype of arthritic synoviocytes. *Proceedings of the National Academy of Sciences*, 103(46):17432–17437, 2006.

- [17] Rosario García-Vicuña, Maria Victoria Gómez-Gaviro, Maria Jesús Domínguez-Luis, Martina K Pec, Isidoro González-Alvaro, Jose María Alvaro-Gracia, and Federico Díaz-González. Cc and cxc chemokine receptors mediate migration, proliferation, and matrix metalloproteinase production by fibroblast-like synoviocytes from rheumatoid arthritis patients. *Arthritis & Rheumatism*, 50(12):3866–3877, 2004.
- [18] Nathan J Zvaifler. Relevance of the stroma and epithelial-mesenchymal transition (emt) for the rheumatic diseases. *Arthritis research & therapy*, 8(3):210, 2006.
- [19] MM Ainola, JA Mandelin, Mikko P Liljeström, TF Li, MV Hukkanen, and YT Konttinen. Pannus invasion and cartilage degradation in rheumatoid arthritis: involvement of mmp-3 and interleukin-1b. *Clin Exp Rheumatol*, 23:644–50, 2005.
- [20] T Pap, I Meinecke, U Müller-Ladner, and S Gay. Are fibroblasts involved in joint destruction? *Annals of the rheumatic diseases*, 64(suppl 4):iv52–iv54, 2005.
- [21] Atsushi Kitani, Noriko Nakashima, Tomomaro Izumihara, Masaki Inagaki, Xu Baoui, Su Yu, Takemasa Matsuda, and Takami Matsuyama. Soluble vcam-1 induces chemotaxis of jurkat and synovial fluid t cells bearing high affinity very late antigen-4. *The Journal of Immunology*, 161(9):4931–4938, 1998.
- [22] Hans P Kiener, Birgit Niederreiter, David M Lee, Esther Jimenez-Boj, Josef S Smolen, and Michael B Brenner. Cadherin 11 promotes invasive behavior of fibroblast-like synoviocytes. *Arthritis & Rheumatism*, 60(5):1305–1310, 2009.
- [23] S Kroesen, AF Widmer, A Tyndall, and P Hasler. Serious bacterial infections in patients with rheumatoid arthritis under anti-tnf- α therapy. *Rheumatology*, 42(5):617–621, 2003.
- [24] RN Maini, PC Taylor, J Szechinski, K Pavelka, J Bröll, G Balint, P Emery, F Raemmen, J Petersen, J Smolen, et al. Double-blind randomized controlled clinical trial

- of the interleukin-6 receptor antagonist, tocilizumab, in european patients with rheumatoid arthritis who had an incomplete response to methotrexate. *Arthritis & Rheumatism*, 54(9):2817–2829, 2006.
- [25] Ravinder N Maini, Ferdinand C Breedveld, Joachim R Kalden, Josef S Smolen, Diana Davis, John D MacFarlane, Christian Antoni, Burkhard Leeb, Michael J Elliott, James N Woody, et al. Therapeutic efficacy of multiple intravenous infusions of anti-tumor necrosis factor α monoclonal antibody combined with low-dose weekly methotrexate in rheumatoid arthritis. *Arthritis & Rheumatism: Official Journal of the American College of Rheumatology*, 41(9):1552–1563, 1998.
- [26] Michael H Weisman. What are the risks of biologic therapy in rheumatoid arthritis? an update on safety. *JOURNAL OF RHEUMATOLOGY-SUPPLEMENT-*, pages 33–38, 2002.
- [27] Jeanne Keffer, Lesley Probert, Haris Cazlaris, Spiros Georgopoulos, Evangelos Kaslaris, Dimitris Kioussis, and George Kollias. Transgenic mice expressing human tumour necrosis factor: a predictive genetic model of arthritis. *The EMBO journal*, 10(13):4025–4031, 1991.
- [28] Rasheena Edmondson, Jessica Jenkins Broglie, Audrey F Adcock, and Liju Yang. Three-dimensional cell culture systems and their applications in drug discovery and cell-based biosensors. *Assay and drug development technologies*, 12(4):207–218, 2014.
- [29] Harris Perlman and Richard M Pope. The synovial lining micromass system: toward rheumatoid arthritis in a dish? *Arthritis & Rheumatism*, 62(3):643–646, 2010.
- [30] Hans P Kiener, Gerald FM Watts, Yajun Cui, John Wright, Thomas S Thornhill, Markus Sköld, Samuel M Behar, Birgit Niederreiter, Jun Lu, Manuela Cernadas, et al. Synovial fibroblasts self-direct multicellular lining architecture and synthetic

- function in three-dimensional organ culture. *Arthritis & Rheumatism*, 62(3):742–752, 2010.
- [31] Šeila Selimović, Jonghyun Oh, Hojae Bae, Mehmet Dokmeci, and Ali Khademhosseini. Microscale strategies for generating cell-encapsulating hydrogels. *Polymers*, 4(3):1554–1579, 2012.
- [32] Beate M Rüger, Tanja Buchacher, Alexander Giurea, Bernd Kubista, Michael B Fischer, and Johannes M Breuss. Vascular morphogenesis in the context of inflammation: Self-organization in a fibrin-based 3d culture system. *Frontiers in Physiology*, 9, 2018.
- [33] Yuhua Zheng, Yvonne Kong, and Edward J Goetzl. Lysophosphatidic acid receptor-selective effects on jurkat t cell migration through a matrigel model basement membrane. *The Journal of Immunology*, 166(4):2317–2322, 2001.
- [34] Corning. *Certificate of Analysis, Corning Matrigel Basement Membrane Matrix Growth Factor Reduced*, 2017.
- [35] Rowan S Hardy, Claudia Hülso, Yingling Liu, Sylvia J Gasparini, Colette Fong-Yee, Jinwen Tu, Shihani Stoner, Paul M Stewart, Karim Raza, Mark S Cooper, et al. Characterisation of fibroblast-like synoviocytes from a murine model of joint inflammation. *Arthritis research & therapy*, 15(1):R24, 2013.
- [36] Saraju P Mohanty and Elias Kougiianos. Biosensors: a tutorial review. *Ieee Potentials*, 25(2):35–40, 2006.
- [37] Pavel Damborský, Juraj Švitel, and Jaroslav Katrlík. Optical biosensors. *Essays in biochemistry*, 60(1):91–100, 2016.
- [38] Klaus B Mogensen and Jörg P Kutter. Optical detection in microfluidic systems. *Electrophoresis*, 30(S1):S92–S100, 2009.

- [39] Hans P Kiener, David M Lee, Sandeep K Agarwal, and Michael B Brenner. Cadherin-11 induces rheumatoid arthritis fibroblast-like synoviocytes to form lining layers in vitro. *The American journal of pathology*, 168(5):1486–1499, 2006.
- [40] G Raschke, S Kowarik, T Franzl, C Sönnichsen, TA Klar, J Feldmann, A Nichtl, and K Kürzinger. Biomolecular recognition based on single gold nanoparticle light scattering. *Nano letters*, 3(7):935–938, 2003.
- [41] WI Goldberg. Dynamic light scattering. *American Journal of Physics*, 67(12):1152–1160, 1999.
- [42] Sai Bi, Xiaoqiang Jia, Jiayan Ye, and Ying Dong. Linear light-scattering of gold nanostars for versatile biosensing of nucleic acids and proteins using exonuclease iii as biocatalyst to signal amplification. *Biosensors and Bioelectronics*, 71:427–433, 2015.
- [43] R Pecora. Dynamic light scattering measurement of nanometer particles in liquids. *Journal of nanoparticle research*, 2(2):123–131, 2000.
- [44] Irving Itzkan, Le Qiu, Hui Fang, Munir M Zaman, Edward Vitkin, Ionita C Ghirvan, Saira Salahuddin, Mark Modell, Charlotte Andersson, Lauren M Kimerer, et al. Confocal light absorption and scattering spectroscopic microscopy monitors organelles in live cells with no exogenous labels. *Proceedings of the National Academy of Sciences*, 104(44):17255–17260, 2007.
- [45] Dakota Watson, Norbert Hagen, Jonathan Diver, Philippe Marchand, and Mirianas Chachisvilis. Elastic light scattering from single cells: orientational dynamics in optical trap. *Biophysical journal*, 87(2):1298–1306, 2004.
- [46] Jason R Wojciechowski, Lisa C Shriver-Lake, Mariko Y Yamaguchi, Erwin Fureder, Roland Pieler, Martin Schamesberger, Christoph Winder, Hans Jurgen Prall, Max

- Sonnleitner, and Frances S Ligler. Organic photodiodes for biosensor miniaturization. *Analytical chemistry*, 81(9):3455–3461, 2009.
- [47] Kang-Jun Baeg, Maddalena Binda, Dario Natali, Mario Caironi, and Yong-Young Noh. Organic light detectors: photodiodes and phototransistors. *Advanced materials*, 25(31):4267–4295, 2013.
- [48] Sandro F Tedde, Johannes Kern, Tobias Sterzl, Jens Furst, Paolo Lugli, and Oliver Hayden. Fully spray coated organic photodiodes. *Nano letters*, 9(3):980–983, 2009.
- [49] Verena Charwat, Michaela Purtscher, Sandro F Tedde, Oliver Hayden, and Peter Ertl. Standardization of microfluidic cell cultures using integrated organic photodiodes and electrode arrays. *Lab on a Chip*, 13(5):785–797, 2013.
- [50] Verena Charwat, Mario Rothbauer, Sandro F Tedde, Oliver Hayden, Jacobus J Bosch, Paul Muellner, Rainer Hainberger, and Peter Ertl. Monitoring dynamic interactions of tumor cells with tissue and immune cells in a lab-on-a-chip. *Analytical chemistry*, 85(23):11471–11478, 2013.
- [51] Eric K Sackmann, Anna L Fulton, and David J Beebe. The present and future role of microfluidics in biomedical research. *Nature*, 507(7491):181, 2014.
- [52] Guisheng Zhuang, Thomas G Jensen, and Jörg P Kutter. Detection of unlabeled particles in the low micrometer size range using light scattering and hydrodynamic 3d focusing in a microfluidic system. *Electrophoresis*, 33(12):1715–1722, 2012.
- [53] Stefan Haeberle and Roland Zengerle. Microfluidic platforms for lab-on-a-chip applications. *Lab on a chip*, 7(9):1094–1110, 2007.
- [54] Nupura S Bhise, João Ribas, Vijayan Manoharan, Yu Shrike Zhang, Alessandro Polini, Solange Massa, Mehmet R Dokmeci, and Ali Khademhosseini. Organ-on-a-chip platforms for studying drug delivery systems. *Journal of Controlled Release*, 190:82–93, 2014.

- [55] Fuyin Zheng, Fanfan Fu, Yao Cheng, Chunyan Wang, Yuanjin Zhao, and Zhongze Gu. Organ-on-a-chip systems: Microengineering to biomimic living systems. *Small*, 12(17):2253–2282, 2016.
- [56] Marshall Fixman. Molecular theory of light scattering. *The Journal of Chemical Physics*, 23(11):2074–2079, 1955.
- [57] David W Hahn. Light scattering theory. *Department of Mechanical and Aerospace Engineering, Florida*, 2006.
- [58] Peter Debye. Light scattering in solutions. *Journal of Applied Physics*, 15(4):338–342, 1944.
- [59] John M Steinke and AP Shepherd. Comparison of mie theory and the light scattering of red blood cells. *Applied optics*, 27(19):4027–4033, 1988.
- [60] PF Mullaney and PN Dean. The small-angle light scattering of biological cells: Theoretical considerations. *Biophysical journal*, 10(8):764, 1970.
- [61] Judith R Mourant, James P Freyer, Andreas H Hielscher, Angelia A Eick, Dan Shen, and Tamara M Johnson. Mechanisms of light scattering from biological cells relevant to noninvasive optical-tissue diagnostics. *Applied optics*, 37(16):2586–3593, 1998.
- [62] Direction of scattered light: www.hyperphysics.phy-astr.gsu.edu.
- [63] Jinjun Zhao, Qingqing Ouyang, Ziyou Hu, Qin Huang, Jing Wu, Ran Wang, and Min Yang. A protocol for the culture and isolation of murine synovial fibroblasts. *Biomedical reports*, 5(2):171–175, 2016.
- [64] Dow Corning. Sylgard 184 silicone elastomer. *Technical Data Sheet*, 2014.

- [65] Effie C Tsilibary and Aristidis S Charonis. The role of the main noncollagenous domain (nc1) in type iv collagen self-assembly. *The Journal of cell biology*, 103(6):2467–2473, 1986.
- [66] I Watanabe and S Okada. Effects of temperature on growth rate of cultured mammalian cells (15178y). *The Journal of cell biology*, 32(2):309–323, 1967.
- [67] Bernard Lorber, Frédéric Fischer, Marc Bailly, Herve Roy, and Daniel Kern. Protein analysis by dynamic light scattering: methods and techniques for students. *Biochemistry and Molecular Biology Education*, 40(6):372–382, 2012.
- [68] Daniel Croft, Peter McIntyre, Auragun Wibulswas, and IJsbrand Kramer. Sustained elevated levels of vcam-1 in cultured fibroblast-like synoviocytes can be achieved by tnf- α in combination with either il-4 or il-13 through increased mrna stability. *The American journal of pathology*, 154(4):1149–1158, 1999.
- [69] Gaël McGill, Akiko Shimamura, Richard C Bates, Robert E Savage, and David E Fisher. Loss of matrix adhesion triggers rapid transformation-selective apoptosis in fibroblasts. *The Journal of cell biology*, 138(4):901–911, 1997.
- [70] Jacob Sode, Ulla Vogel, Steffen Bank, Paal Skytt Andersen, Marianne Kragh Thomsen, Merete Lund Hetland, Henning Loch, Niels HH Heegaard, and Vibeke Andersen. Anti-tnf treatment response in rheumatoid arthritis patients is associated with genetic variation in the nlrp3-inflammasome. *PLoS One*, 9(6):3e100361, 2014.
- [71] J Beuthan, U Netz, O Minet, Annerose D Klose, AH Hielscher, A Scheel, J Henniger, and G Müller. Light scattering study of rheumatoid arthritis. *Quantum Electronics*, 32(11):945–952, 2002.
- [72] Nicholas J Schork. Personalized medicine: time for one-person trials. *Nature*, 520(7549):609–611, 2015.

- [73] Mario Rothbauer, David Wartmann, Verena Charwat, and Peter Ertl. Recent advances and future applications of microfluidic live-cell microarrays. *Biotechnology advances*, 33(6):948–961, 2015.

A. Materials and Methods

Python Program Code

```
import statistics
import os
import getdata
import time
if not os.path.exists('Mean'):
    os.makedirs('Mean') Directory=sorted(os.listdir('Rohdaten_Cont'))
    Filenamemedian=('Mean_continuous.dat')
if os.path.exists(os.path.join('Mean',Filenamemedian)):
    os.remove(os.path.join('Mean',Filenamemedian))
Fm=open(os.path.join('Mean',Filenamemedian),"a+")
Fm.write('Date'+'\t'+ 'FLS1 ch1'+'\t'+ 'FLS1 ch5'+'\t'+ 'FLS2 ch1'+'\t'+ 'FLS2 ch5'+
'\t'+ 'TNF1 ch1'+'\t'+ 'TNF1 ch5'+'\t'+ 'TNF2 ch1'+'\t'+ 'TNF2 ch5'+'\t'+ 'Matrigel
ch1'+'\t'+ 'Matrigel ch5'+'\t'+ 'ohne ch1'+'\t'+ 'ohne ch5'+'\n')
for y in Directory:
    Filenames=sorted((os.listdir(os.path.join('Rohdaten_Cont',y))),key=lambda s: s.lower())
    Power=[(83.4,67.4),(83.3,66.4),(82.4,68.8),(81.9,68.1),(82.1,67.3)]
    Powerday=Power[int(y)]
    t=[]
    for x in Filenames:
        ch1=[]
        ch5=[]
        Datum=[]
        ch1pos=[]
        ch5pos=[]
        F=open(os.path.join('Rohdaten_Cont',y,x),'r')
        Lines=F.readlines()[1:]
        getdata.getdata(Lines,ch1,ch5,t)
        for z in ch1:
            if 'ohne' in x.split('_')[0]:
                ch1pos.append(z)
            else:
                if z>0:
                    ch1pos.append(z)
```

```

for z in ch5:
    if 'ohne' in x.split('-')[0]:
        ch5pos.append(z)
    else:
        if z>0:
            ch5pos.append(z)
ch1med=statistics.mean(ch1pos)
ch5med=statistics.mean(ch5pos)
if 'FLS' in x.split('-')[0]:
    if 'FLS1' in x.split('-')[0]:
        Datum=y
        ch1med2=ch1med*Powerday[1]/Powerday[0]
        Fm.write(Datum+'\t'+str(ch1med2)+'\t'+str(ch5med)+'\n')
    if 'FLS2' in x.split('-')[0]:
        Datum=y
        ch1med2=ch1med*Powerday[1]/Powerday[0]
        Fm.write(Datum+'\t'+'\t'+'\t'+str(ch1med2)+'\t'+str(ch5med)+'\n')
if 'TNF' in x.split('-')[0]:
    if 'TNF1' in x.split('-')[0]:
        Datum=y
        ch1med2=ch1med*Powerday[1]/Powerday[0]
        Fm.write(Datum+'\t'+'\t'+'\t'+'\t'+'\t'+str(ch1med2)+'\t'+str(ch5med)+'\n')
    if 'TNF2' in x.split('-')[0]:
        Datum=y
        ch1med2=ch1med*Powerday[1]/Powerday[0]
        Fm.write(Datum+'\t'+'\t'+'\t'+'\t'+'\t'+'\t'+'\t'+'\t'+str(ch1med2)+'\t'+
        str(ch5med)+'\n')
if 'M' in x.split('-')[0]:
    if 'M' in x.split('-')[0]:
        Datum=y
        ch1med2=ch1med*Powerday[1]/Powerday[0]
        Fm.write(Datum+'\t'+'\t'+'\t'+'\t'+'\t'+'\t'+'\t'+'\t'+'\t'+str(ch1med2)+
        '\t'+str(ch5med)+'\n')
if 'ohne' in x.split('-')[0]:
    Datum=y
    ch1med2=ch1med*Powerday[1]/Powerday[0]

```

```
ohnechipsmean=ch1med2+ch5med/2
Fm.write(Datum+'\t'+'\t'+'\t'+'\t'+'\t'+'\t'+'\t'+'\t'+'\t'+'\t'+'\t'+
str(ch1med2)+'\t'+str(ch5med)+'\n')
F.close()
Fm.close()
```

Python Program Code "getdata"

```
def getdata(Lines,ch1,ch5,t):
    i=0
    for x in Lines:
        i=(i+1)
        j=i/10
        t.append(j)
        ch1.append(float(x.split(' ')[2]))
        ch5.append(float(x.split(' ')[6]))
```